2027

Y-1797

MASTER

TIME FLUCTUATIONS OF TEMPERATURE IN A MAGNETOHYDRODYNAMIC PLASMA

E. M. Murray

UNION CARBIDE CORPORATION
NUCLEAR DIVISION
OAK RIDGE Y-12 PLANT

operated for the ATOMIC ENERGY COMMISSION under U. S. GOVERNMENT Contract W-7405 eng 26

UNION CARBIDE
OAK RIDGE Y-12 PLANT
P. O. Box Y
OAK RIDGE, TENNESSEE 37830

DISTRIBUTION OF THIS DOCUMENT IS UNLIMITED

DISCLAIMER

This report was prepared as an account of work sponsored by an agency of the United States Government. Neither the United States Government nor any agency Thereof, nor any of their employees, makes any warranty, express or implied, or assumes any legal liability or responsibility for the accuracy, completeness, or usefulness of any information, apparatus, product, or process disclosed, or represents that its use would not infringe privately owned rights. Reference herein to any specific commercial product, process, or service by trade name, trademark, manufacturer, or otherwise does not necessarily constitute or imply its endorsement, recommendation, or favoring by the United States Government or any agency thereof. The views and opinions of authors expressed herein do not necessarily state or reflect those of the United States Government or any agency thereof.

DISCLAIMER

Portions of this document may be illegible in electronic image products. Images are produced from the best available original document.

Printed in the United States of America. Available from
National Technical Information Service
U.S. Department of Commerce
5285 Port Royal Road, Springfield, Virginia 22151
Price: Printed Copy $3.00; Microfiche $0.95

This report was prepared as an account of work sponsored by the United States Government. Neither the United States nor the United States Atomic Energy Commission, nor any of their employees, nor any of their contractors, subcontractors, or their employees, makes any warranty, express or implied, or assumes any legal liability or responsibility for the accuracy, completeness or usefulness of any information, apparatus, product or process disclosed, or represents that its use would not infringe privately owned rights.

Reference to a company or product name does not imply approval or recommendation of the product by Union Carbide Corporation or the U S Atomic Energy Commission to the exclusion of others that may meet specifications.

UC-37 Y-1797

TIME FLUCTUATIONS OF TEMPERATURE IN A MAGNETOHYDRODYNAMIC PLASMA

E. M. Murray

Oak Ridge Y-12 Plant

P.O. Box Y, Oak Ridge, Tennessee 37830

operated for the U.S. ATOMIC ENERGY COMMISSION
by UNION CARBIDE CORPORATION–NUCLEAR DIVISION
under Contract W-7405-eng-26

Date Issued - January 24, 1972

This report is based on a study by the author as partial fulfillment of requirements for the degree of Master of Science in Physics from The University of Tennessee.

Work covered in this report was performed at The University of Tennessee Space Institute, Tullahoma, Tennessee.

NOTICE

This report was prepared as an account of work sponsored by the United States Government. Neither the United States nor the United States Atomic Energy Commission, nor any of their employees, nor any of their contractors, subcontractors, or their employees, makes any warranty, express or implied, or assumes any legal liability or responsibility for the accuracy, completeness or usefulness of any information, apparatus, product or process disclosed, or represents that its use would not infringe privately owned rights.

DISTRIBUTION OF THIS DOCUMENT IS UNLIMITED

DISTRIBUTION

Atomic Energy Commission-ORO

Keller, C. A.
Zachry, D. S., Jr

Oak Ridge Gaseous Diffusion Plant

Jordan, R. G.
Wilcox, W. J., Jr

Oak Ridge Y-12 Plant

Bernander, N. K.
Briscoe, O. W.
Burditt, R. B.
Burkhart, L. E.
Denny, A. (2)
Ellingson, R. D.
Foulk, D. L.
Hemphill, L. F.
Jackson, V. C.
Jones, F. W.
Kahl, K. G.
Keith, Alvin
Kite, H. T.
Long, P. J.
Mason, D. L.
McLendon, J. D.
Mitchel, G. W.
Murray, E. M. (20)
Oliphant, G. W.
Smith, R. D.
Snow, S. G.
Stoner, H. H.
Trotter, T. C.
Weathersby, W. E.
Wesley, R. L.
Yaggi, W. J.
Y-12 Central Files (5)
Y-12 Central Files (master copy)
Y-12 Central Files (route)
Y-12 Central Files (Y-12RC)

Paducah Gaseous Diffusion Plant

Winkel, R. A.

In addition, this report is distributed in accordance with the category UC-37, Instruments, as given in the "USAEC Standard Distribution Lists for Unclassified Scientific and Technical Reports", TID-4500.

ACKNOWLEDGEMENTS

The author greatly appreciates the technical guidance and patience given throughout the experimental investigation by Dr. J. B. Dicks, Jr. and Dr. J. K. Koester of The University of Tennessee Space Institute. He is also grateful for the assistance given by the members of the Magnetohydrodynamic Group at the Space Institute in setting up the experiment and operating the generator.

ABSTRACT

An experimental investigation of the temperature of a potassium-seeded magnetohydrodynamic plasma has been performed. The main means of obtaining temperature measurements incorporated an apparatus which contains two photomultiplier tubes that sensed light intensity fluctuations from the plasma. The plasma temperature, Hall voltage, and static pressure parameters of a Hall generator have been analyzed for functional dependance of one parameter on another.

Two separate temperature measurement techniques have been utilized in this experimental investigation: (1) measuring the electrical conductivity of the plasma from the Hall channel from which a temperature measurement was obtained and (2) incorporating the ratio of the outputs of both the photomultiplier tubes and a mathematical derivation from Planck's blackbody radiation law to obtain a temperature determination. Voltage signals from equipment sensing the plasma parameters have been recorded and the autocorrelation and crosscorrelation functions have been determined.

TABLE OF CONTENTS

LIST OF TABLES

LIST OF FIGURES

FIGURE PAGE

CHAPTER I

INTRODUCTION

The basic principle of a linear magnetohydrodynamic (MHD) generator is that a magnetic field is set perpendicular to the direction of motion of a moving plasma. This pattern is identical to the situation of a solid conductor cutting magnetic field lines. Thus, an electromotive force is set up by the plasma. An external return path is provided thereby producing a flow of current and an extraction of power from the generator. Electrical power is gained by reducing the velocity of the plasma. This action extracts directed energy from the flowing plasma and converts it into electrical energy in the external load (external return path).

The mechanism of primary importance in the MHD generator is the plasma. A plasma is a gas which is ionized sufficiently that a small amount of charge separation can take place, but the plasma itself is approximately neutral even though its principle constituents are charged ions and electrons. Significant amounts of energy are needed to produce and maintain such a medium which results in a rise in temperature. A question that follows is just what is the temperature of the plasma. This question forms the basis of the work described in this thesis.

An experimental determination of the plasma temperature is desirable to better understand the overall operation of the MHD generator. One way this temperature measurement would clarify an understanding of the MHD generator would be to simplify the calculations of the velocity and density of the plasma from the equations of continuity and state. This temperature measurement would facilitate the calculation of the degree of ionization undergone by potassium in the plasma flow. In this study, the potassium in a potassium hydroxide (KOH)-methyl alcohol seed solution is the main source of electrons in the plasma. A major clarification that would result from the temperature measurement would be a simplified calculation of the electrical conductivity (σ) of the MHD plasma(1).[1]

Finally, there exists another question that could be answered by the continuous measurement of the plasma temperature. This question is concerned with the possibility that the plasma temperature as it fluctuates with time affects other generator parameters such as static pressure and Hall voltage.

---

[1] Numbers in parentheses refer to similarly numbered references in the bibliography.

CHAPTER II

MAGNETOHYDRODYNAMIC EXPERIMENTAL LABORATORY

I. EXPERIMENTATION FACILITY

The experimental investigation was accomplished in The University of Tennessee Space Institute (UTSI) MHD Laboratory. The MHD Laboratory configuration is shown in Figure 1. The laboratory is divided into two main sections—the test facility and the instrumentation and control room. The principal equipment in the test facility is the combustor-nozzle used to produce the MHD plasma, the MHD generator, and the magnet. The support equipment consists of the igniter and fuel system, a cooling water system, a load bank, a magnet power supply (welders), a diffuser, and an exhaust duct. The control room instrumentation contains a 24-channel oscillograph, a 12-channel oscillograph, a four-channel tape recorder, a seven-channel tape recorder, a plywood panel mounting approximately 100 meters, a polaroid camera, and a 70-mm self-incrementing camera. The MHD generator, diffuser, and exhaust duct are insulated from ground.

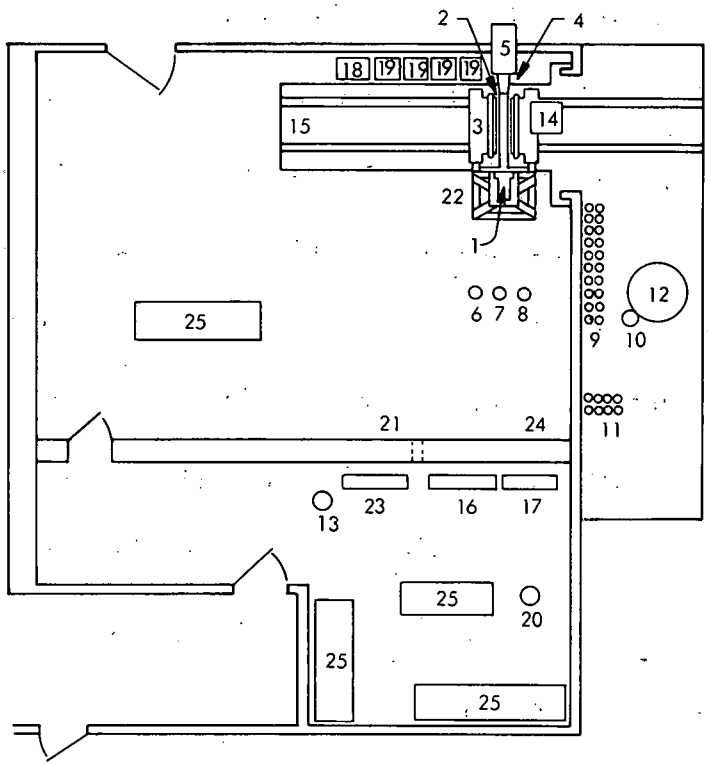

1. Combustor
2. MHD Generator
3. Electromagnet
4. Diffuser
5. Exhaust Duct
6. Gaseous Hydrogen for Igniter
7. Compressed Air for Igniter
8. Seed Tank
9. Gaseous Oxygen Tanks
10. Fuel Tank
11. Gaseous Nitrogen Tanks
12. Water Tank
13. Gaseous Argon Tank
14. Phototubes and Optics Container
15. Magnet Well
16. Instrumentation and Control Panels
17. Meter Panel
18. Load Bank
19. Magnet Power Supply (16 Welders)
20. Cameras
21. Observation Port
22. Shunt Panel
23. Temperature Measurement Instrumentation
24. Personnel Protection Wall
25. Work Bench

FIGURE 1

ARRANGEMENT OF THE MHD LABORATORY

II. COMBUSTOR-NOZZLE

The source of power for the MHD generator is a partially ionized plasma produced by burning a mixture of kerosene and gaseous oxygen in a rocket-type combustion chamber. In this study, the seeding agent is potassium hydroxide dissolved in methyl alcohol. Several seed concentrations are used during this experiment. The most concentrated solution is composed of 20 per cent KOH, by weight, in the alcohol. This 20 per cent seed concentration yields a 1 per cent pure potassium concentration in the combustion chamber. The seeding material is necessary because, at the existing flame temperature of 3300 degrees Kelvin (a theoretical determination), very little ionization takes place without the presence of such a material as potassium. The potassium provides sufficient ions for satisfactory plasma conductivity.

The physical dimensions of the cylindrical combustion chamber are 18 centimeters in diameter and 36 centimeters in length. A converging subsonic nozzle section upstream of the throat accomplishes the transition from the circular cross section of the combustor to the rectangular cross section of the MHD generator. A nominal exit Mach number of 1.6 is produced from the contoured supersonic section diverging from 5.1 to 7.6 centimeters at the throat to 5.1 by 10.0 centimeters at the outlet of the nozzle. The approximate

flow rate at the throat is 0.7 kilogram per second. The exhaust velocity at the outlet is approximately 1700 meters per second.

III. MHD GENERATOR

The MHD generator which is used for the temperature measurement experiment is known as a Hall generator. This type of MHD generator consists of conducting walls that are at an angle of 90 degrees to the axis of flow of the MHD plasma. The Hall MHD generator is schematically shown in Figure 2. The MHD generator consists of three main sections: an upstream transition section, an active generator section, and a downstream transition section. The active generator section consists of 60 elements or electrodes machined from electrolytic copper; its high thermal capacity allows the existence of a heat sink and a generator operation for a period of 10 to 12 seconds. Experimental data are taken through an optical window through a port in one of the generator elements. Each element consists of two sections which are insulated and joined together at the center of the element side walls by nonmagnetic screws. Ceramic fiber paper of 0.05 centimeter thickness is used to electrically insulate the adjoining generator elements. Elements are integrally interconnected for structural rigidity by nonmagnetic screws which are insulated by ceramic spacers. The MHD generator is supported by two stainless steel rails which are insulated from the channel by 6.4-millimeter-thick

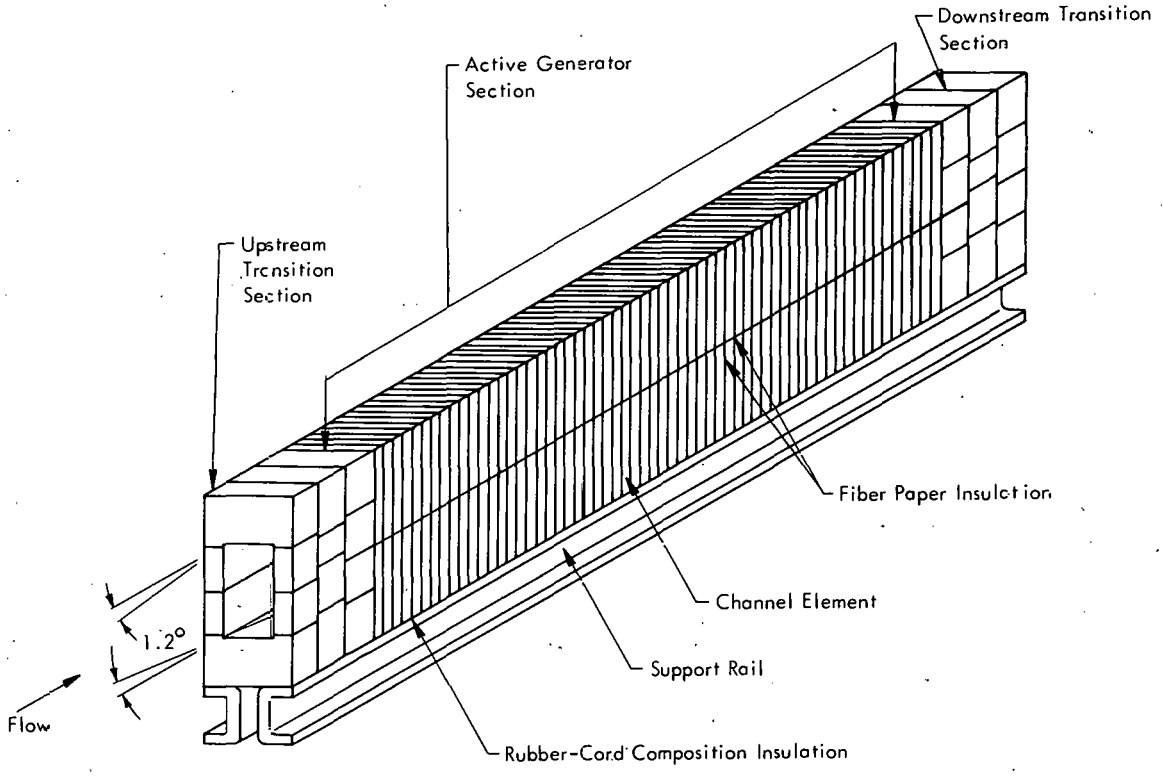

FIGURE 2

SCHEMATIC OF THE MHD HALL GENERATOR

rubber and cord composition strips. Each rail is attached to the generator by stainless steel fasteners electrically insulated by ceramic and Teflon insulators.

The approximate overall dimensions of the MHD generator are: 9.5 centimeters in width, 20.5 centimeters in height, and 122 centimeters in length. The plasma flow passage of the channel diverges from an inlet area of approximately 52 square centimeters to an outlet area of approximately 78 square centimeters. The angle of divergence of the walls of the flow passage perpendicular to the E field of the magnet is 1.2 degrees while the walls perpendicular to the B field remain parallel.

The MHD generator is attached to the combustor-nozzle by an adapter flange which is rigidly fixed. The MHD generator physically expands downstream, when heated, and freely slides on the composition insulation on the support rails. The support rails are rigidly attached to a support stand which rests in the magnet well, between the magnet poles. This support stand rests on and is electrically insulated from the magnet by rubber composition pads.

During this experiment, the temperatures of the channel walls after a 10-second firing are: at the upstream B walls, approximately 573 degrees Kelvin; at the downstream B walls, approximately 473 degrees Kelvin; at the E walls, approximately 100 degrees Kelvin less. The B walls reach the highest temperature due to their relatively smaller mass.

The Hall channel is set up and instrumented to measure the electrical conductivity of the MHD plasma during the plasma temperature measuring experiment. The electrical connections to the MHD generator are shown schematically in Figure 3. An external voltage is applied between the first three and the last three elements of the Hall channel. No magnetic field is applied to the MHD generator. The flow of electric current and of the plasma is approximately parallel. Equipotential surfaces perpendicular to the plasma flow are produced by the elements of the MHD channel. Potential differences between the elements of the channel exist. Electrical connections are placed at varied intervals along the channel and these voltages are measured during each MHD generator test. The flow of current between the first three and the last three elements of the Hall channel are likewise measured during each generator test. The electrical conductivity (σ) of the plasma is an extremely useful parameter for the calibration of the plasma temperature experiment. The electrical conductivity has a high degree of dependence on the plasma temperature(2).

IV. MAGNET

The magnet that is used with the MHD generator is a water-cooled electromagnet that can produce a magnetic field of 20 kilogauss across a gap of four inches. The magnet consists of a C-frame core which is a one-piece,

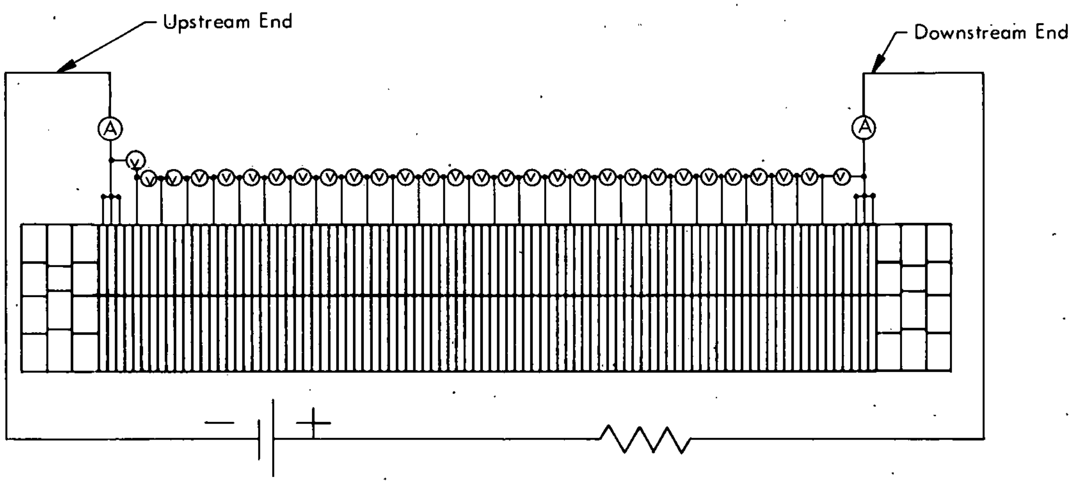

FIGURE 3

CONDUCTIVITY INSTRUMENTATION SCHEMATIC
OF THE HALL CHANNEL

low-carbon-steel weldment. There are four coils (indirectly cooled copper foil windings) for each pole. The approximate total weight of the magnet is 11,500 kilograms. Full field strength is produced by the energizing coils when the magnet is supplied with 125 kilowatts of power at approximately 120 volts.

V. SUPPORT EQUIPMENT

The igniter system consists of a hydrogen-air pilot flow and a spark plug. The hydrogen-air pilot blows passed the spark plug, which ignites it, into the combustion chamber.

Pressure-actuated Annin valves control the sequence and flow of fuel, seed mixture, and oxygen for the combustor. In addition, these valves control the sequence and flow of hydrogen and compressed air for the igniter. A low-pressure nitrogen system controls solenoid valves which actuate the Annin valves. An automatic timer properly sequences the opening and closing of the solenoid valves to accomplish satisfactory ignition and combustion.

Regulation of the pressure in the supply tanks controls the flow rates of the liquids; pressure regulators in the delivery lines control the gaseous flow rates. All flow rates are preset prior to a test run.

The combustor, nozzle, magnet, and exhaust duct are all water cooled. The cooling system operates at a total flow rate of approximately 1140 liters per minute.

The load bank has the function of dissipating the electrical power, up to a maximum of 100 kilowatts, generated by the MHD channel. The load bank is air cooled and is composed of 252 1.4-ohm heater element resistors. The individual 1.4-ohm resistors are connected together to produce the desired resistance load.

Power for the electromagnet coils is produced by 16 direct current (DC) welders connected in series which supply a total of 2100 amperes at 120 volts.

The diffuser for the plasma leaving the MHD generator consists of a welded stainless steel structure which has diverging walls. This diffuser is rigidly attached to the MHD generator by an adapter flange and is so constructed that the exiting plasma is at atmospheric pressure.

The exhaust duct contains a water spraying fixture which cools the plasma to reduce the electrical conductivity. The cooling water spray collects much of the particulate combustion products. The exhaust duct is insulated from ground since it is in contact with the plasma and therefore attains a high electrical potential.

VI. INSTRUMENTATION

There are several parameters which are of primary interest in the overall understanding of the operation of the diagonal, conducting-wall MHD

generator. These parameters include: total current, electrode current, total voltage, voltage between elements, temperature of the generator walls, and static pressure along the generator walls. Primary parameters of the combustor are: fuel flow rate, alcohol-KOH mixture flow rate, oxygen flow rate, total chamber pressure, and oxygen line pressure.

Most of the electrical measurements are made by mounted panel meters. Data measured by these meters do not require fast response time instrumentation. The panel meter data are recorded by a polaroid camera and a 70-mm camera, which takes exposures at two-second intervals.

Panel meters with 10-millivolt and 50-millivolt full-scale deflections and an accuracy of 2 per cent of full scale are used. Full-scale deflection of a meter can be made to represent a wide range of input voltages due to the technique of calibration of applying a known input signal and adjusting a variable resistance in the meter circuit. The meters are connected from the instrumentation and control room by a cluster of identified leads in a cableway to a group of banana plugs mounted on a phenolic panel board in the test facility. Leads run from the banana plugs on the panel board to electrical contacts of interest on the MHD generator.

There are 45 meters, which have a full-scale deflection of 50 millivolts, that are usually used as voltmeters. There is a 100-kilohm-to-10-megohm variable resistor in series with and a 47-ohm damping resistor

(to eliminate oscillations in the meter movement) in parallel with each meter.

There are 40 meters, each individually connected in parallel across separate current shunts, which have a full-scale deflection of 10 millivolts and serve as ammeters. A zero-to-two-kilohm variable resistor is connected in series from the meter to the current shunt. No damping resistor is necessary.

The current shunts are rigidly mounted to two separate phenolic panel boards. The first panel board mounts 40 current shunts which are each rated at from 5 to 100 amperes and 0.5 milliohm. The second mounts 26 current shunts which are each rated at from 0.2 to 5 amperes and 0.1 ohm.

The meters, wires, and shunts are well insulated from ground since their electrical connections are directly connected to the MHD generator and therefore they assume the potential of the element of the generator to which they are connected. The phenolic shunt panel boards and the meter panel are of nonconducting materials. The insulation resistance of the electrical connection cable is rated at 3000 volts (DC).

There are some MHD generator parameters that require continuous monitoring. Galvanometer oscillographs are used to perform this task. The parameter signals are input to the oscillograph galvanometers which enable the recording of data on photosensitive data paper. The result is a continuous display of data thereby allowing the correlation of several parameters at a

particular instant of time. Other important advantages of the galvanometer oscillographs are: (1) the improvement of the frequency response, over the meter movement, and (2) the ability to measure low-level signals with the aid of DC amplifiers.

Temperature measurements of the walls of the MHD generator are performed by Chromel-Alumel thermocouples which are implanted in the generator at various locations. These thermocouple readouts are displayed on ten pyrometers mounted on the meter panel.

Strain-gage pressure transducers are used to measure the static pressure inside the generator channel at several locations, the total pressure inside the combustor, and the pressure inside the fuel and oxygen lines. These strain gages are balanced and calibrated, based on information supplied by the manufacturer, with an electronic gage control device. Low-frequency oscillograph galvanometers are electrically connected directly to the strain-gage outputs.

A Meriam indicating flowmeter is utilized to measure the flow rate of oxygen to the combustor. A mercury manometer is used to measure the pressure drop across the thin-plate, sharp-edge orifice of the Meriam meter. The manufacturer supplies the calibration curves for the orifice. A change-of-pressure (ΔP) measurement is recorded by the oscillograph from a ΔP strain-gage transducer.

Turbine flowmeters are utilized to measure the flow rates of the kerosene and the alcohol-potassium hydroxide mixture. These turbine flowmeters produce alternating current (AC) pulses proportional to the rate of flow of the liquid. A panel meter and an oscillograph galvanometer receive a DC-millivolt signal. This DC signal is converted from the AC frequency by an electronic flowrate indicator.

VII. TEMPERATURE EXPERIMENT APPARATUS

The temperature of the MHD plasma is measured by an apparatus which consists of a light collimator, a container which holds an optical system and two photomultiplier tubes, and an optical fiber which transmits the light from the collimator to the container.

The light collimator (refer to Figure 4) is a stainless steel tubular fixture which is approximately 15 centimeters long, 1.27 centimeters in diameter at one end, and 1.9 centimeters in diameter at the other end. The smaller end of the collimator threads into an MHD channel element. The collimator-channel element assembly is shown in Figure 5. The larger-diameter end of the collimator contains an optical window and threaded fitting which secures the optical window and mounts one end of the optical fiber. The light collimator and optical fiber mounting fixture contain through their entire length a centered 3.2-millimeter-diameter hole. The diameter of this hole is the same as the

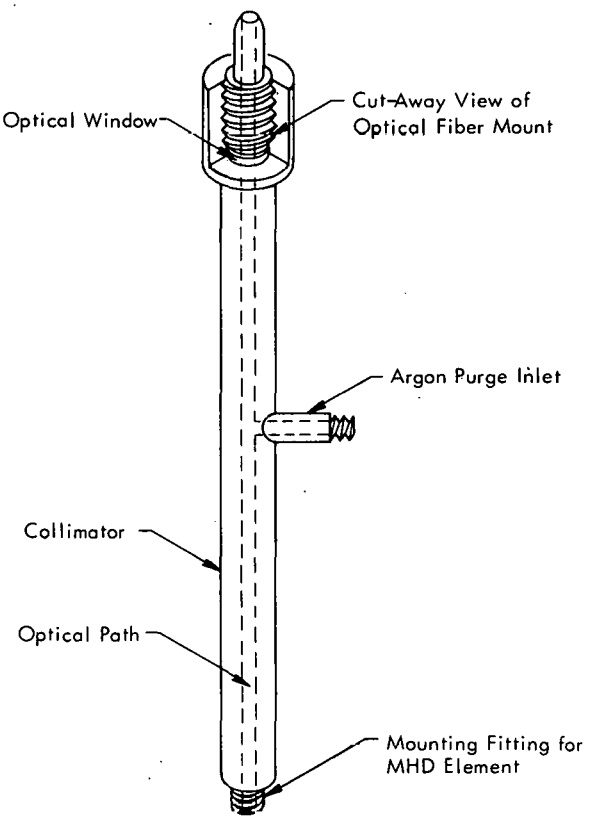

FIGURE 4

OPTICAL COLLIMATOR

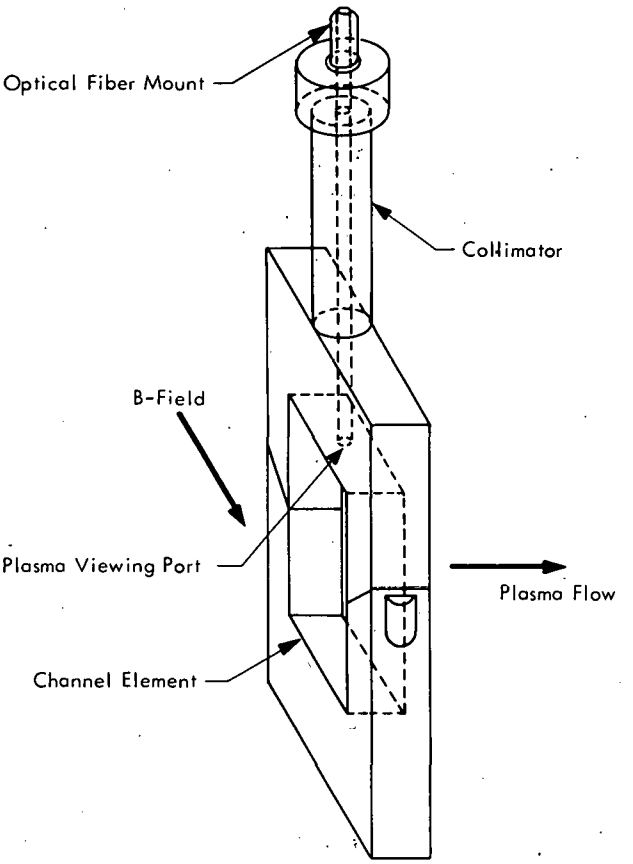

FIGURE 5

COLLIMATOR AND MHD
CHANNEL ELEMENT

external diameter of the optical fiber. The collimator contains a fitting which allows the installation of an argon purge system. This system keeps the optical window clean of any solid by-product deposits from the MHD plasma during a test run. The length of the collimator is large compared with the internal diameter of the optical window to ensure that the spectral radiance(3) of the plasma source is not a function of the distance.

The container which holds the optical system and photomultiplier tubes is open at the top, is constructed of stainless steel, and is approximately 76 centimeters long, 58 centimeters wide, and 17.8 centimeters deep. This container is mounted on top and to the side of the magnet. Figure 6 is a drawing of the experiment's container. There are two main sections to this container. The first section contains two areas. One area contains the optical platform and the optical components and the second area consists of a work space to make it possible to remove the resistor strings and photomultiplier tubes. These two areas are connected by four mild-steel tubes of two different diameters (5.1 cms. and 7.62 cms.) which contain the resistor strings and photomultiplier tubes. These two areas are optically isolated from the outside by opaque fiber board and sealed at the joints by black photographic masking tape. Both areas and the interior of the mild steel tubes are constantly purged with dry nitrogen before, during, and after a MHD generator run. The second main section of the container, which remains open to the outside, is used to hold

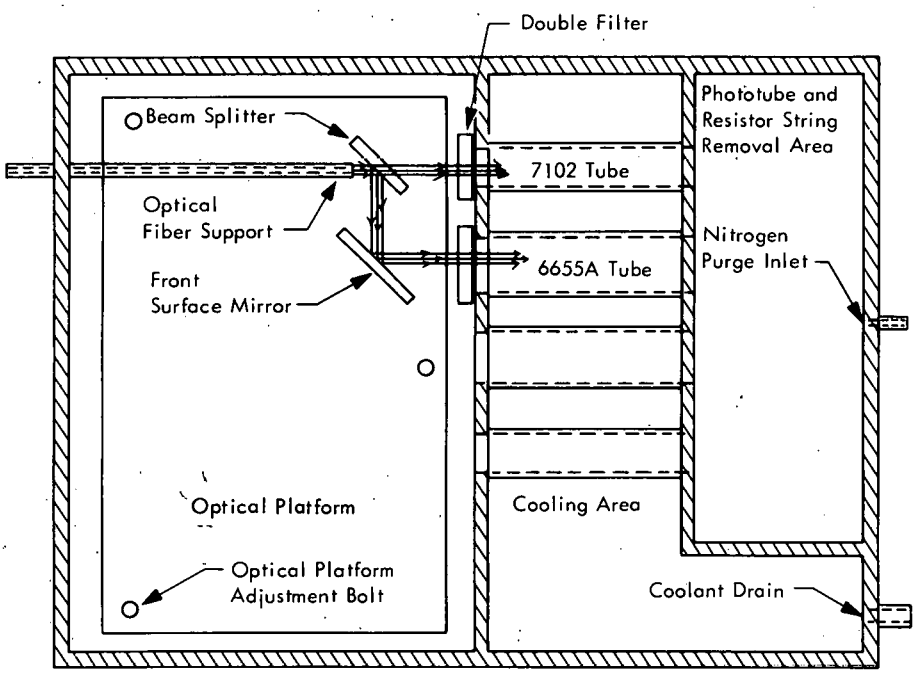

FIGURE 6

TEMPERATURE EXPERIMENT CONTAINER AND OPTICAL PATHS

methyl alcohol and solid carbon dioxide (Dry Ice) to cool the photomultiplier tubes. This second section is sealed from the first by welding. The mild steel tubes traverse the cooled section and therefore their exterior walls are immersed in the alcohol-Dry Ice solution. The phototubes are enclosed by mild-steel rather than stainless steel tubes due to the high permeability of the mild steel. This permeability reduces the magnetic field effect of the magnet and the earth's magnetic field on the photomultiplier tubes.

The optics of the experiment consist of a half-silvered mirror (beam splitter) and a front-surfaced mirror. These mirrors are mounted in frames, secured to an aluminum optical bench plate, which can be adjusted to facilitate alignment. The optical fiber, supported by a tubular fixture, is brought to within approximately 1.27 centimeters of the beam splitter. The beam is split so that one set of rays moves toward the first photomultiplier tube while the second set of rays moves toward the front surface mirror. The front surface mirror deflects the second set of rays toward the second photomultiplier. A double set of filters are mounted between each photomultiplier tube and its respective set of rays. The combination of filters is dependent on the wavelength of light that is desired to enter each photomultiplier tube. The first photomultiplier tube is filtered by a 693-millimicron second-order interference filter plus a Type 21 Wratten filter and senses the desired wavelength of 694 millimicrons. The second photomultiplier tube is filtered by a 582-millimicron

second-order interference filter plus a Type 21 Wratten filter and senses the desired wavelength of 583 millimicrons.

The first photomultiplier tube is an RCA Type 7102 and the second, an RCA Type 6655A. The dynodes of the photomultiplier tubes receive the appropriate voltages from resistor strings that were made for the experiment. Figures 7 and 8 are electrical schematics of the resistor strings of the 7102 and 6655A phototubes, respectively. The high voltage (1200 volts DC) for the two phototubes comes from a power supply located in the control room through an appropriately rated cable. Figure 9 is the schematic for the phototube-instrumentation connections. The signal from the 7102 photomultiplier tube goes through a preamplifier (for impedance match of the cable), a cable from the test facility to the control room, a signal amplifier, and to a high-frequency (8000-hertz) galvanometer in the oscillograph. The signal from the 6655A photomultiplier tube goes through a cable from the test facility to the control room, a signal amplifier, and to a high-frequency (8000-hertz) galvanometer in the oscillograph.

The optical fiber transmits the spectral radiance of the MHD plasma from the collimator to the optics in the experiment's container. The optical fiber is approximately 91 centimeters long and has an external diameter of 3.2 millimeters. This optical fiber consists of a bundle of noncoherently arranged 250-micron-diameter fibers which will transmit light in the wavelength range

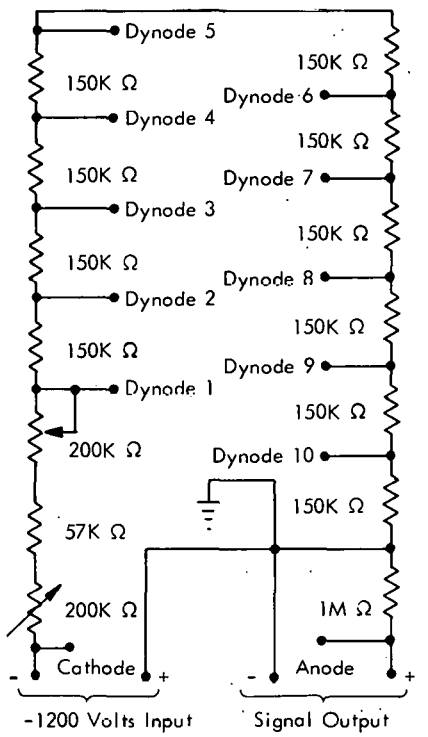

FIGURE 7

SCHEMATIC OF THE PHOTOTUBE
7102 RESISTOR STRING

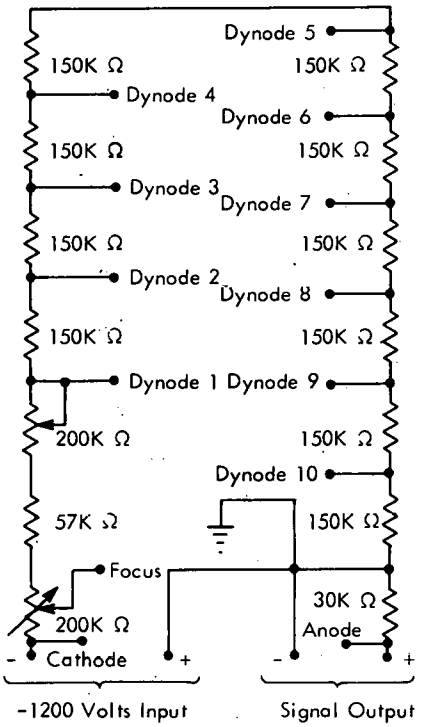

FIGURE 8

SCHEMATIC OF THE PHOTOTUBE
6655A RESISTOR STRING

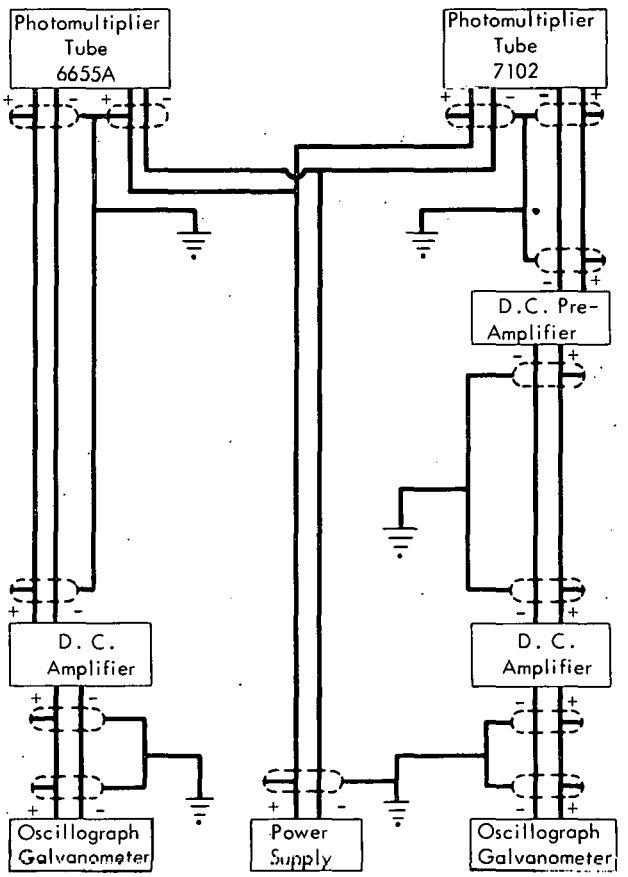

FIGURE 9

SCHEMATIC OF THE TEMPERATURE MEASUREMENT ELECTRONICS

of from 400 to 1100 millimicrons. Approximately 27 per cent of the original spectral radiance of the MHD plasma is dissipated in the 91-centimeter section of the optical fiber used(4).

VIII. MHD GENERATOR TEST PROCEDURE

The major steps involved in a MHD generator test, including the temperature measurement experiment, are enumerated in the following outline. All the instrumentation calibration is performed immediately following installation of the MHD generator:

1. The water, fuel, and seed tanks are inspected and filled if necessary.
2. The electrical sequencing of the pressure-actuated Annin valves is checked.
3. The combustor, magnet, and exhaust duct cooling water system is checked.
4. An igniter test firing is conducted.
5. The pressures for the gaseous storage tanks are checked.
6. The nitrogen purge for the temperature measurement experiment container is activiated.
7. The cooling section of the temperature measurement experiment container is filled with methyl alcohol and solid carbon dioxide.

8. The oscillographs and the pressure transducers are calibrated.
9. The seed and fuel tanks are pressurized to predetermined values.
10. The magnet power supplies (welders) are activated.
11. The combustor, magnet, and exhaust duct water cooling system is activated.
12. The argon purge for the optical collimator is activated.
13. The magnetic field of the magnet is adjusted to full strength.
14. The electronic sequencing mechanism is activated.
15. Data are taken by the automatic instrumentation during the MHD generator test.
16. The MHD channel is purged with nitrogen after the test.
17. The magnetic field strength of the magnet is reduced to the minimum value.
18. The magnet power supply is deactivated.
19. The water cooling system is deactivated.
20. The seed and fuel tanks are depressurized.

The combustor operates most efficiently at the parameter flow rates of:

Kerosene	0.16 kilogram per second
Oxygen	0.57 kilogram per second
Alcohol-KOH Solution	0.06 kilogram per second
Total	0.79 kilogram per second

The theoretical approximate MHD generator and plasma parameters that exist at these flow rates are(5):

Chamber Pressure	31 newtons per square centimeter atmospheric
Hall Parameter	1.0
Mach Number	1.5
Velocity	1500 meters per second
Conductivity	17 mhos per meter
Plasma Temperature	2700 degrees Kelvin

CHAPTER III

TEMPERATURE MEASUREMENT TECHNIQUES AND CALIBRATION

I. METHODS OF MEASURING TEMPERATURE AND CALIBRATION

The temperature of the MHD plasma is determined by two different measurement techniques: (1) a conductivity-temperature measurement, and (2) a photomultiplier tube ratio temperature measurement. The conductivity-temperature measurement technique is performed with the aid of a computer program(6) that calculates the electrical conductivity of the MHD plasma. This measurement procedure is independent of the photomultiplier tube techniques and aides in the development of the photomultiplier tube ratio temperature measurement procedure. The photomultiplier tube ratio temperature measurement procedure depends on the ratio of the direct outputs of both photomultiplier tubes.

II. CONDUCTIVITY-TEMPERATURE MEASUREMENT

The conductivity-temperature measurement procedure is performed with the aid of a computer program which performs the theoretical calculation of the MHD plasma conductivity. The computer program yields data that

makes possible the production of plasma conductivity versus plasma temperature curves. It is possible to experimentally measure the conductivity of the plasma; therefore, the plasma temperature is obtainable from these curves.

The actual theory(7) by which the computer program performs the conductivity calculation of the MHD plasma consists of the use of the equation:

$$\sigma = en_e\mu, \tag{1}$$

where σ represents the electrical conductivity of the plasma, e the electronic charge, n_e the electron density, and μ the electron mobility. The equilibrium constant (K) for the ionization of atoms is determined by the Saha equation:

$$K = \frac{n_e n_i}{n_o} = \frac{2g_i}{g_o} \frac{(2\pi mkT)^{3/2}}{h^3} e^{-\left[\frac{eV_i}{hT}\right]}, \text{ or} \tag{2}$$

which results to a form to yield the electron density,

$$n_e = \frac{n_e}{n_i} \frac{2g_i}{g_o} \frac{(2\pi mkT)^{3/2}}{h^3} e^{-\left[\frac{eV_i}{hT}\right]}, \tag{3}$$

where k represents the Boltzmann constant, h Planck's constant, V_i the ionization potential of potassium, m and e the electronic mass and charge respectively, T the temperature in degrees Kelvin, the n's the densities, and the g's the statistical weights. The subscripts e, i, and o denote electrons, ions, and neutral atoms, respectively. The electron mobility is determined by the equation:

$$\mu = \frac{4\pi e}{3m} \int_0^\infty F(v) \left(\frac{d}{dv}\right) \left(\frac{v^3}{v_t}\right) dv, \qquad (4)$$

where e represents the electronic charge, m the electronic mass, v the electronic velocity, v_t the total collision frequency, and F(v) the electron velocity distribution function. Equation 4 is correct when no magnetic field is present, which is the case when the MHD channel is instrumented for conductivity runs.

Execution of the computer program(6) requires the use of experimentally measured values of several of the MHD plasma parameters. These required parameters included the oxygen flow rate, fuel flow rate, alcohol-KOH seed flow rate, percentage of KOH in the alcohol-KOH seed solution, the total chamber pressure, and the static pressure existing at the electrode through which the plasma was viewed. The computer program yields, among other data, the conductivity and temperature of the MHD plasma which exists at a particular instant of time. The enthalpy of the MHD plasma which is calculated theoretically by the computer is artificially lowered in the computer program by subtracting from it a constant(8). The data output from the computer thus consists of a lower conductivity versus a lower temperature. A successive lowering of the enthalpy yields lower and lower output data that enables the production of a calibration curve of plasma conductivity versus temperature for a specific set of plasma parameters. It is now possible to determine the temperature of the plasma for a specific set of plasma parameters provided the conductivity of the plasma is known, and this

conductivity is in the range of the calibration curve. Figure 10 is an example of one of the plasma conductivity versus temperature curves. This curve is plotted to fit the data points using the exponential least-squares-fit mathematical technique.

The electrical conductivity of the plasma is experimentally measured by using the Hall MHD generator in the conductivity configuration (refer to Figure 3, Page 10). The theory involved in this measurement is contained in Ohm's law:

$$\vec{J} = \sigma\vec{E}, \text{ or} \tag{5}$$

$$\sigma = \frac{\vec{J}}{\vec{E}} = \frac{\vec{I}}{\vec{E}\cdot A} = \frac{\vec{I}}{A}\frac{N\ell}{V} = \frac{N\ell}{A}\frac{I}{V}, \tag{6}$$

where $\vec{J}$ represents the current density, $\vec{E}$ the electrical field strength, $\vec{I}$ the total current flowing through the MHD generator during a run, A the cross-sectional area of the MHD channel at the point at which the plasma was viewed, ℓ the thickness of each electrode plus the insulation thickness, N the number of electrodes that are of interest, and V the voltage across the N number of electrodes. Inserting the constant values into Equation 6 gives:

$$\sigma = 19.74\frac{I}{V}, \tag{7}$$

where and I and V are experimentally measured from the Hall channel during each generator run.

It is therefore possible to determine the temperature of the MHD plasma for a given set of parameters provided there exists an experimental

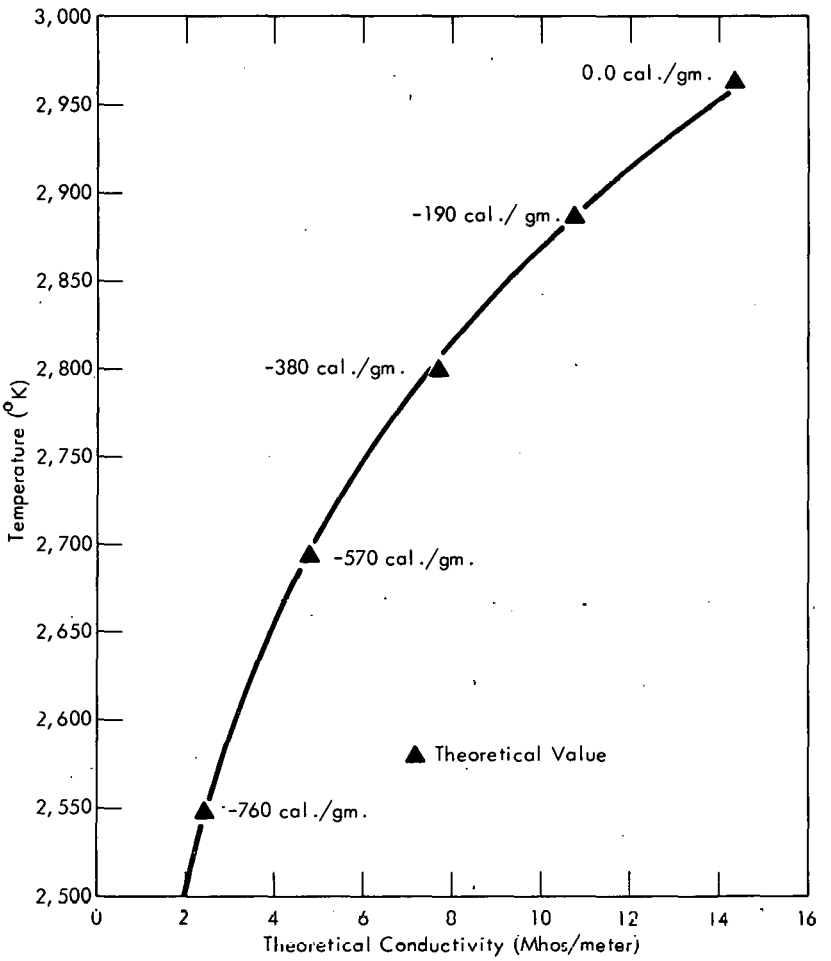

FIGURE 10

REPRESENTATIVE THEORETICAL CONDUCTIVITY VERSUS TEMPERATURE CURVE

measurement of the plasma conductivity and a corresponding conductivity-versus-temperature curve.

III. PHOTOMULTIPLIER TUBE RATIO TEMPERATURE MEASUREMENT

The photomultiplier tube ratio temperature measurement technique is the main temperature measurement procedure that is used for this experiment. The theory for this procedure will be discussed in Chapter IV. This measurement procedure is developed with the aid of the information obtained from the previously discussed conductivity-temperature measurement technique.

It is necessary to determine the response of the phototubes in the temperature measurement apparatus. This is performed with the aid of a standard temperature reference source and some means of measuring the temperature of this reference. The standard temperature reference source that is used is a tungsten ribbon filament lamp that can produce a maximum true temperature of over 3000 degrees Kelvin. The apparatus that is used to measure the brightness temperature of the tungsten ribbon filament is an optical pyrometer. The optical pyrometer that is used is a Leeds and Northrup Model 8636-C. This pyrometer is factory calibrated for blackbody conditions and can measure brightness temperatures in the range of

1348 through 4573 degrees Kelvin. The pyrometer operates on the disappearing filament principle.

The spectral radiance of tungsten of the ribbon filament is not identical to that of a true blackbody; therefore, a correction of the pyrometer temperature measurement is incorporated into the final measurement data. Figure 11 is a graph of the correction from brightness temperature (measured by the pyrometer) to a real temperature(9).

There is a direct dependence of the temperature of the tungsten ribbon filament on the amount of electric current that flows through the ribbon filament. A small apparatus, which is schematically shown in Figure 12, was built to allow adjustment of the amount of current that flows through the tungsten ribbon filament. This current measuring device consists of a current shunt, a potentiometer, and a 50-millivolt full-scale meter movement. This apparatus also mounts the tungsten ribbon filament lamp and provides an input for the lamp power supply. The tungsten ribbon filament requires from 30 to 44 amperes of electrical current to produce the brightness temperatures in the range of interest. The power supply that is used is a welder from the magnet power supply. The electrical current from the power supply flows through an on-off switch, the current shunt, a fuse, and to the tungsten ribbon filament lamp. The current shunt is rated at from 0 to 50 amperes and will produce correspondingly from 0 to 100 millivolts. The millivolt signal

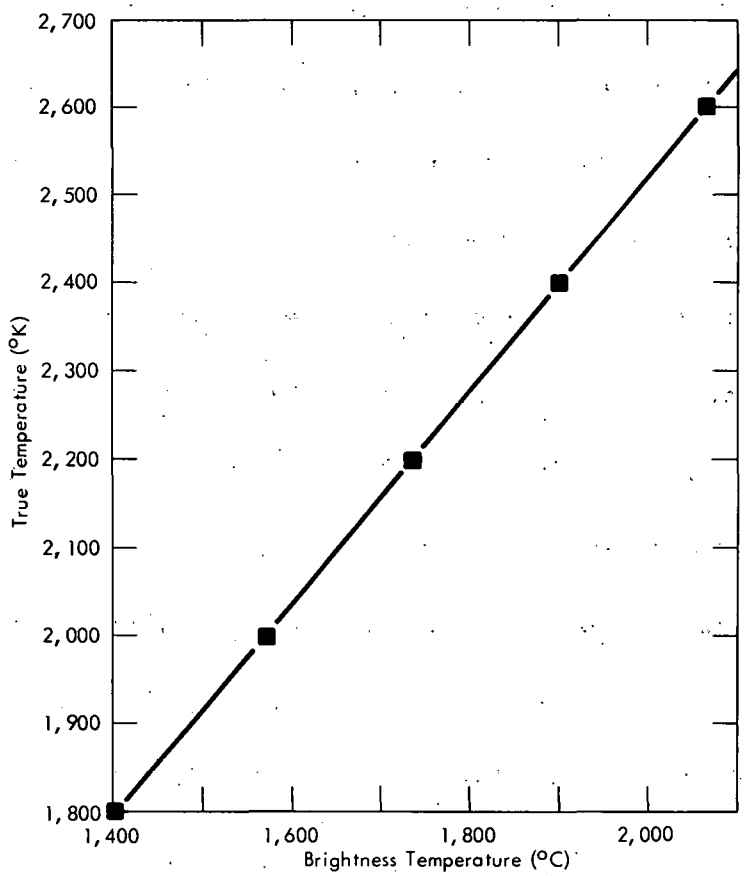

FIGURE 11

LEAST SQUARES CORRECTION CURVE OF THE BRIGHTNESS TEMPERATURE TO THE TRUE TEMPERATURE OF THE TUNGSTEN RIBBON FILAMENT STANDARD

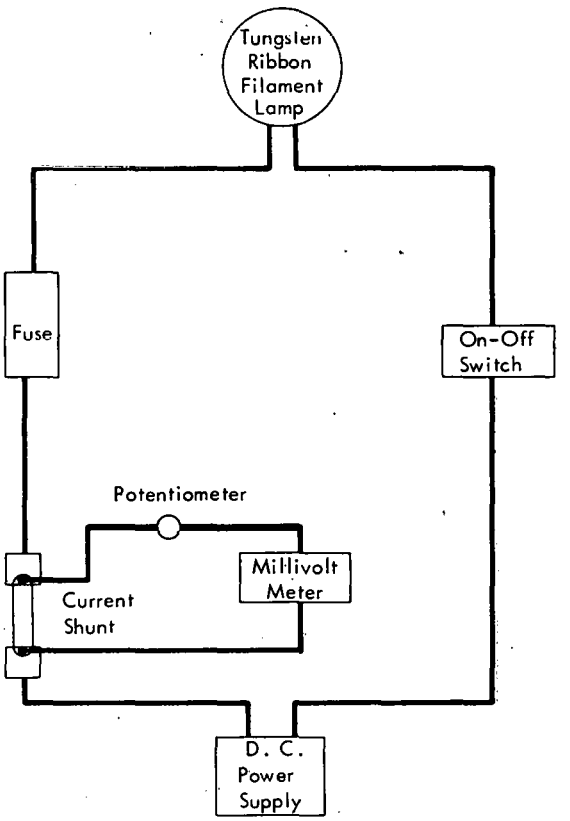

FIGURE 12

SCHEMATIC OF THE FILAMENT CURRENT MEASUREMENT APPARATUS

from the shunt is attenuated by the potentiometer before it reaches the meter movement. The meter movement is adjusted by the potentiometer to sense from 30 to 44 amperes of current that flows through the shunt. The meter scale is incremented in percentages of full-scale deflection; therefore, the actual current flowing through the shunt is not measured. It is therefore possible to obtain a true temperature measurement (using the correction curve) of the tungsten ribbon filament corresponding to a percentage of full-scale deflection of the meter. The optical pyrometer is used to measure the temperature of the tungsten ribbon filament. These pyrometer measurements are performed at each five-per cent increment between the meter positions of 50 and 75 per cent of full scale. The standard deviation of these pyrometer measurements is seven degrees Kelvin.

It is then possible to calibrate the photomultiplier tube temperature measurement electronics. This calibration is accomplished by adjusting the entire photomultiplier tube temperature measurement apparatus as if it is actually sensing the spectral radiance of the MHD plasma, except that the collimator is positioned to view the center of the tungsten ribbon filament. The tungsten filament lamp power supply is activated and is adjusted to produce a desired percentage of full-scale meter deflection. This meter deflection corresponds to a true filament temperature, which produces a certain spectral radiance that results in a particular DC signal from the phototube.

Finally, a characteristic deflection of the galvanometer is produced in the oscillograph. The deflection of the galvanometer therefore corresponds directly to the true temperature of the tungsten ribbon filament.

Calibration data for a particular photomultiplier tube is produced by adjusting the temperature of the tungsten ribbon filament and recording the corresponding galvanometer deflections. The standard deviation of the galvanometer deflections for a calibration is ± 0.05 centimeters. This calibration data is used to determine a constant necessary to solve the equation developed in the next chapter. The ratio of the two output deflections of the galvanometers connected to the photomultiplier tubes is calculated and is used in conjunction with the equations which are developed and discussed in the following chapter.

CHAPTER IV

THEORETICAL INVESTIGATION

I. RATIO TEMPERATURE MEASUREMENT

The basis of the ratio temperature measurement is the 7102 and 6655A photomultiplier tube outputs, which are dependent on the spectral radiance of two certain precise wavelengths of light from the plasma. The wavelengths of light that are permitted to be sensed by the photomultiplier tubes were those of two potassium KI lines. The KI line pair(10) that is observed in this experiment is the 583-millimicron 5^2D-4^2P and the 694-millimicron 6^2S-4^2P. The filter system of the 7102 photomultiplier tube has a band pass of from 688 to 698 millimicrons and therefore passes the 694-millimicron KI line. The filter system of the 6655A photomultiplier tube has a band pass of from 577 to 587 millimicrons and therefore passes the 583-millimicron KI line.

The theory that this temperature determination is constructed around is Planck's blackbody radiation law, which is described by the equation:

$$E(\lambda,T) = \frac{C_1 \lambda^{-5}}{e^{C_2/\lambda T} - 1}, \tag{8}$$

where $C_1 = 3.741 \times 10^{-4}$ watts $-\mu^2$, $C_2 = 1.438 \times 10^4$ μ - ° K, λ represents the wavelength of light, T the temperature in degrees Kelvin, and $E(\lambda, T)$ the emissive power of a blackbody per unit wavelength(11). For this particular case it is possible to write Equation 8 as:

$$E(\lambda,T) = \frac{C_1 \lambda^{-5}}{\exp\left[C_2/\lambda T\right]}, \tag{9}$$

since the value of the exponential is so much larger than unity. It is possible to make the mathematical statement:

$$R \propto E(\lambda,T)\, \epsilon(\lambda,T), \tag{10}$$

where R represents the oscillograph deflection corresponding to the spectral radiance of one of the KI lines and $\epsilon(\lambda, T)$ the emissivity of the tungsten. The emissivity factor is necessary since the tungsten ribbon filament is not a true blackbody. From Equation 10 the extensions are written as:

$$R_a = f_a\, E(\lambda_a,T)\, \epsilon(\lambda_a,T), \tag{11}$$

where R_a represents the oscillograph deflection that is associated with the 7102 photomultiplier tube and f_a, a constant that is considered as a calibration constant, and:

$$R_b = f_b\, E(\lambda_b,T)\, \epsilon(\lambda_b,T), \tag{12}$$

where R_b represents the oscillograph deflection that is associated with the 6655A photomultiplier tube and f_b, a constant that is considered as a calibration factor. Taking the ratio of Equations 11 and 12, produces the equation:

$$\frac{E(\lambda_a, T)}{E(\lambda_b, T)} = \frac{f_b}{f_a} \frac{R_a}{R_b} \frac{\epsilon(\lambda_b, T)}{\epsilon(\lambda_a, T)} . \tag{13}$$

The form of Planck's blackbody radiation law (Equation 9) that is associated with each of the two photomultiplier tubes produces the ratio equation:

$$\frac{E(\lambda_a, T)}{E(\lambda_b, T)} = \frac{\lambda_b^5}{\lambda_a^5} \frac{\exp\left[C_2/\lambda_b T\right]}{\exp\left[C_2/\lambda_a T\right]}, \text{ or} \tag{14}$$

$$\frac{E(\lambda_a, T)}{E(\lambda_b, T)} = \frac{\lambda_b^5}{\lambda_a^5} \exp\left[\frac{C_2}{\lambda_b T} - \frac{C_2}{\lambda_a T}\right]. \tag{15}$$

Equating Equations 15 and 13 results in the equation:

$$\frac{f_b}{f_a} \frac{R_a}{R_b} \frac{\epsilon(\lambda_b, T)}{\epsilon(\lambda_a, T)} = \frac{\lambda_b^5}{\lambda_a^5} \exp\left[\frac{C_2}{\lambda_b T} - \frac{C_2}{\lambda_a T}\right], \text{ or} \tag{16}$$

$$\ln\left[\frac{\lambda_a^5}{\lambda_b^5} \frac{f_b}{f_a} \frac{R_a}{R_b} \frac{\epsilon(\lambda_b, T)}{\epsilon(\lambda_a, T)}\right] = \frac{C_2}{T}\left[\frac{1}{\lambda_b} - \frac{1}{\lambda_a}\right], \text{ or} \tag{17}$$

$$T = \frac{C_2 \left(\frac{1}{\lambda_b} - \frac{1}{\lambda_a} \right)}{\ln \left[\frac{\lambda_a}{\lambda_b}^5 \frac{f_b}{f_a} \frac{R_a}{R_b} \frac{\epsilon(\lambda_b, T)}{\epsilon(\lambda_a, T)} \right]}. \tag{18}$$

The wavelengths, λ_a and λ_b, correspond to the wavelengths of the KI lines that affect the 7102 and 6655A photomultiplier tubes, respectively. These wavelength values are $\lambda_a = 0.694$ micron and $\lambda_b = 0.583$ micron and produce the value:

$$\left(\frac{\lambda_a}{\lambda_b} \right)^5 = 2.390.$$

The emissivity(8) ratio in Equation 18 is calculated at the maximum calibration temperature (T = 2490° K) and produces the result:

$$\frac{\epsilon(\lambda_b, T)}{\epsilon(\lambda_a, T)} = 1.036.$$

The emissivity ratio varies only slightly over the entire temperature calibration range.

Equation 18, with the calculated ratios, can be written as:

$$T = \frac{C_2 \left(\frac{1}{\lambda_b} - \frac{1}{\lambda_a} \right)}{\ln \left[2.476 \frac{R_a}{R_b} \frac{f_b}{f_a} \right]}, \text{ or} \tag{19}$$

$$T = \frac{3948}{\ln \left[2.476 \frac{R_a}{R_b} \frac{f_b}{f_a} \right]} \text{° K}. \tag{20}$$

The factor, f_b/f_a, is the ratio of the constant calibration factors from both photomultiplier tubes. The value of this ratio is determined by a calibration of the photomultiplier tubes and the following procedure: A calibration of a photomultiplier tube produces a T minimum (1850° K) corresponding to an R minimum, and a T maximum (2490° K) corresponding to an R maximum. An extension of Equation 10 results in the ratio equation:

$$\frac{R_{max.}}{R_{min.}} = \frac{E\left(\lambda, T_{max.}\right)}{E\left(\lambda, T_{min.}\right)} \frac{\epsilon\left(\lambda, T_{max.}\right)}{\epsilon\left(\lambda, T_{min.}\right)}, \text{ or} \tag{21}$$

$$\frac{R_{max.}}{R_{min.}} = \frac{\epsilon\left(\lambda, T_{max.}\right)}{\epsilon\left(\lambda, T_{min.}\right)} \exp\left[\frac{C_2}{\lambda}\left(\frac{1}{T_{min.}} - \frac{1}{T_{max.}}\right)\right], \text{ or} \tag{22}$$

$$\lambda = \frac{C_2\left(\frac{1}{T_{min.}} - \frac{1}{T_{max.}}\right)}{\ln\left[\frac{R_{max.}}{R_{min.}} \frac{\epsilon\left(\lambda, T_{min.}\right)}{\epsilon\left(\lambda, T_{max.}\right)}\right]} = \lambda_{eff.}, \tag{23}$$

where $\lambda_{eff.}$ represents the effective wavelength of radiation that is sensed by the photomultiplier tube during a particular calibration. The $\lambda_{eff.}$ calculation is necessary because the filtering system in front of each photomultiplier tube is not perfect. The actual ratio of f_b and f_a (f_b/f_a) is determined from

Equation 13; but, in terms of $\lambda_{eff.}$ and with T equal to 2490 degrees Kelvin, yields the equation:

$$\frac{f_b}{f_a} = \frac{R_b}{R_a} \frac{E\left(\lambda_{a_{eff.}}, T\right)}{E\left(\lambda_{b_{eff.}}, T\right)} \frac{\epsilon\left(\lambda_a, T\right)}{\epsilon\left(\lambda_b, T\right)} , \tag{24}$$

where R_b/R_a represents the ratio of the oscillograph outputs, from the photomultiplier tubes, at the temperature of 2490 degrees Kelvin.

The only term that now remains unknown in Equation 20 is R_a/R_b, which is the result of the experimental data taken during each generator test run. The final equations therefore used for this temperature measurement are(12):

$$T = \frac{3948}{\ln\left[5.89 \frac{R_a}{R_b}\right]} \,^\circ K, \tag{25}$$

for the calibration when the optical window was completely clear, and

$$T = \frac{3948}{\ln\left[3.36 \frac{R_a}{R_b}\right]} \,^\circ K, \tag{26}$$

for the calibration when the optical window was slightly fogged.

II. CORRELATION OF RANDOM DATA

Several parameters of the MHD generator and plasma exist that are thought to somehow be dependent upon each other. The parameters that are

investigated include the static pressure, the Hall voltage, and the plasma temperature. These parameters are investigated by using the technique of random data analysis(13). The particular analysis procedures that are used in the investigation are the autocorrelation and crosscorrelation functions of the parameters of interest. There also exists a question of whether or not the fluctuations of the plasma temperature occur at a particular frequency.

The autocorrelation function for random data characterizes the general interdependence of the values of the data at one particular time on the values at another particular time. The autocorrelation function, $R_x(\tau)$, is depicted in equation form as:

$$R_x(\tau) = \lim_{T \longrightarrow \infty} \frac{1}{T} \int_0^T x(t)\, x(t+\tau)\, dt, \tag{27}$$

where, $R_x(\tau)$ is always a real-valued even function which has a maximum value at $\tau = 0$.

What actually occurs in the autocorrelation of a random data signal is described in the following sentences: A random data signal is delayed by a specific time interval of τ seconds, known as a lag time. The delayed signal and the original signal are multiplied together at any particular instant of time. The instantaneous product of the original and delayed signals is averaged over the sampling time. This procedure yields what is known

as the autocorrelation estimate, $\hat{R}_x(\tau)$, which is displayed in equation form as:

$$\hat{R}_x(\tau) = \frac{1}{T} \int_0^T x(t)\ x(t+\tau)\ dt. \tag{28}$$

The crosscorrelation function, $R_{xy}(\tau)$, for two sets of random data characterizes the general interdependence of the values of one set of data on the other. The crosscorrelation function is depicted in equation form as:

$$R_{xy}(\tau) = \lim_{T \longrightarrow \infty} \frac{1}{T} \int_0^T x(t)\ y(t+\tau)\ dt, \tag{29}$$

where, $R_{xy}(\tau)$ is always a real-valued function and it can be either positive or negative. If $R_{xy}(\tau) = 0$, then x(t) and y(t) are uncorrelated.

What actually occurs in the crosscorrelation of two random data signals is described in the following sentences: The first signal, x(t), is delayed relative to the second signal, y(t), by a specific time interval of τ seconds. The value of y(t), at any instant of time, is multiplied by the value of x(t) that has occurred τ seconds before. The instantaneous product of the undelayed and the delayed signals is averaged over the sampling time. This procedure yields what is known as the crosscorrelation estimate, $\hat{R}_{xy}(\tau)$, which is displayed in equation form as:

$$\hat{R}_{xy}(\tau) = \frac{1}{T} \int_0^T x(t)\ y(t+\tau)\ dt. \tag{30}$$

CHAPTER V

EXPERIMENTAL RESULTS

I. INTRODUCTION

The experimental data were taken using the Hall MHD generator in the conductivity configuration. The collimator of the photomultiplier tube temperature measurement apparatus was attached to and viewed the plasma through Electrode 20 throughout the experiment. Four welders of the power supply system were connected across the Hall channel to enable the conductivity measurements of the MHD plasma. The external load line consisted of a one-ohm resistance (for the purpose of safety) located at the load bank during the experiment.

It was desirable to manipulate a combustor parameter to lower the temperature of the plasma. The oxygen flow rate was the combustor parameter that resulted in being the safest to adjust and obtain the required temperature lowering effect. It was therefore possible to obtain a plasma temperature operating range of approximately 500 degrees Kelvin. A total of four separate alcohol-KOH seed concentrations were used to observe their effect on the temperature of the plasma.

Data were accumulated from a total of 27 generator test runs. Table I displays the run number, per cent of KOH in the alcohol-KOH seed concentration, and the oxygen flow rate for these 27 generator test runs. The test run numbers are not sequential because either the generator misfired or a data recording device malfunctioned; consequently, no data were recorded for the corresponding test run.

Random data signals were recorded and analyzed for a total of nine generator test runs. Autocorrelation and crosscorrelation comparisons were performed on the photomultiplier tube signal outputs, chamber pressure, and Hall voltage.

II. EXPERIMENTAL RESULTS

Experimental data were recorded to supply the necessary information for the two temperature measurement techniques and for the random data analysis. The following sections discuss the techniques and generator and plasma parameters that were used and involved in this data acquisition.

Conductivity-Temperature Measurement

The data that were required for the conductivity-temperature measurement procedure included the current, I, flowing through the generator and the voltage, V, that existed across Electrodes 16 through 24 of the generator at a particular instant of time. The voltage and current data that were used

TABLE I

MHD GENERATOR TEST HISTORY CORRESPONDING TO INITIAL EXPERIMENTAL PARAMETERS

Run Number	Seed Concentration (%)	Oxygen Flow Rate (kg./sec.)
547	8.7	0.545
548	8.7	0.449
549	8.7	0.428
550	8.7	0.369
551	10.5	0.563
552	10.5	0.513
553	10.5	0.488
554	10.5	0.419
555	10.5	0.369
556	10.5	0.509
557	20.0	0.468
558	20.0	0.523
559	20.0	0.472
560	20.0	0.438
561	20.0	0.359
562	20.0	0.558
563	20.0	0.545
564	20.0	0.478
575	20.0	0.531
576	20.0	0.481
577	20.0	0.429
579	2.5	0.595
580	2.5	0.510
581	2.5	0.492
582	2.5	0.469
583	2.5	0.376
585	2.5	0.552

were recorded at 10 seconds into the generator test run. The MHD generator operated relatively stable at this 10-second point in the test run. The current was measured by an oscillograph galvanometer that was electrically connected to a current shunt attached in series with the generator. The current shunt produced a millivolt signal that actuated the oscillograph galvanometer. The voltage was measured by panel meters that were connected across every third electrode down the channel, except for Electrodes 16 through 24 which were each connected across a meter. A 70-millimeter camera photographed these panel meters at 10 seconds into the generator test run. A graph was plotted for each set of run data of electrode number versus accumulated channel voltage at that electrode. A linear least squares fit was calculated and drawn to the data points which corresponded to Electrodes 16 through 24. The voltage across Electrodes 16 through 24 was then extracted from this graph.

Table II displays the current, voltage, calculated conductivity from Equation 7, the plasma temperature from the previously mentioned conductivity-temperature calibration curves, and the combustor loss. These temperature values represent approximate plasma temperatures that existed and corresponded to the experimentally measured conductivity values. Table III reports most of the data necessary for the previously mentioned computer program to calculate the data required to produce the conductivity-temperature calibration curves. These necessary data included the oxygen flow rate (refer

TABLE II

CONDUCTIVITY-TEMPERATURE MEASUREMENT DATA

Run Number	Current (amperes)	Voltage (volts)	Conductivity (mhos/meter)	Temperature (° K)	Combustor Loss (calories/gram)
547	15.00	27.6	10.7	2707	-485
548	11.25	29.1	7.6	2532	-385
549	6.25	29.4	4.2	2474	-417
550	2.50	24.0	2.0	2306	-178
551	15.00	27.0	11.0	2717	-498
552	16.25	29.4	10.9	2689	-509
553	10.25	30.3	6.7	2535	-588
554	8.00	28.8	5.5	2514	-381
555	4.50	27.6	3.2	2401	-196
556	15.00	30.0	9.9	2640	-572
557	18.80	26.7	13.9	2656	-396
558	17.50	27.0	12.8	2671	-513
559	17.00	30.6	11.0	2564	-476
560	10.00	27.3	7.2	2527	-403
561	2.50	21.0	2.3	2303	-197
562	20.00	27.0	14.6	2731	-545
563	22.25	28.5	15.4	2734	-534
564	22.25	28.5	15.4	2652	-395
575	22.20	29.4	14.9	2733	-477
576	16.25	30.3	10.6	2670	-697
577	11.25	30.3	7.3	2559	-587
579	8.75	30.9	5.6	2720	-515
580	8.75	28.8	6.0	2707	-509
581	6.25	28.5	4.3	2593	-575
582	3.75	27.9	2.6	2547	-637
583	1.25	21.3	1.1	2455	-317
585	10.00	45.0	4.4	2680	-734

TABLE III

MHD PLASMA AND GENERATOR DATA REQUIRED FOR EXECUTION OF COMPUTER PROGRAM

Run Number	Fuel Flow Rate (kg./sec.)	Seed Flow Rate (kg./sec.)	Total Chamber Pressure (newtons/cm.2)	Static Pressure at Electrode 20 (newtons/cm.2)
547	0.142	0.073	33.2	9.4
548	0.149	0.074	29.5	8.4
549	0.151	0.074	27.9	7.9
550	0.160	0.072	25.8	7.2
551	0.134	0.063	32.4	9.5
552	0.142	0.067	31.5	9.4
553	0.149	0.068	31.6	9.3
554	0.151	0.070	29.8	9.3
555	0.156	0.072	27.9	8.9
556	0.146	0.070	25.0	8.5
557	0.156	0.051	32.9	9.5
558	0.160	0.056	31.5	9.4
559	0.157	0.059	29.8	9.0
560	0.165	0.063	28.0	8.6
561	0.166	0.064	25.6	8.1
562	0.139	0.060	24.8	9.6
563	0.149	0.063	25.0	9.6
564	0.158	0.066	25.2	9.6
575	0.131	0.059	31.1	9.8
576	0.123	0.060	28.1	9.8
577	0.139	0.068	28.1	9.6
579	0.139	0.072	33.5	9.9
580	0.132	0.072	31.2	9.8
581	0.139	0.074	30.0	9.3
582	0.144	0.075	27.8	8.8
583	0.144	0.077	25.4	8.2
585	0.131	0.074	25.3	9.8

to Table I, Page 50), fuel flow rate, seed flow rate, seed concentration (refer to Table I), total chamber pressure, and the static pressure existing at Electrode 20.

Some of the data from Table II (Page 52) was plotted in Figure 13. This data showed the relationship between the temperature determinations from the conductivity-temperature measurement, the experimentally determined conductivity, and the corresponding combustor loss undergone by the generator combustor during a particular test run. The data was plotted with aid of four different symbols each of which designated one of the four seed concentrations used during the experiment. The curves drawn on the figure group the plotted parameters with the various seed concentrations. The graph verified that as the temperature decreased the conductivity also decreased and the conductivity increased as the seed concentration increased for a given temperature. The graph also displayed that generally as the temperature and conductivity increased the combustor loss also increased.

The oxygen flow rate was decreased to produce a decrease in plasma temperature. This oxygen decrease affected the other parameters of the combustor (refer to Table III) in the following manner: (1) the fuel flow rate increased, (2) the seed flow rate increased slightly, (3) the total chamber pressure decreased, and (4) the Electrode 20 static pressure decreased.

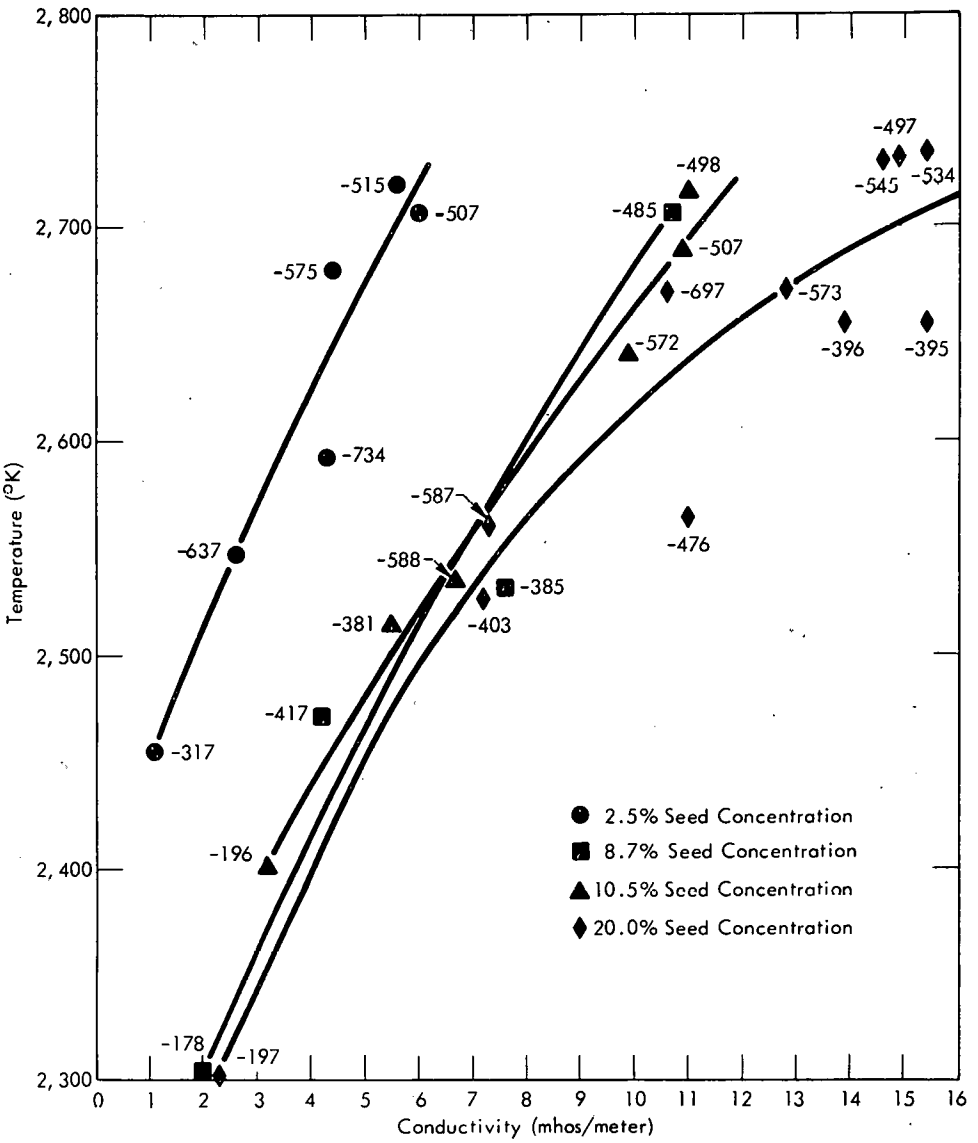

FIGURE 13

COMPARISON OF CONDUCTIVITY-TEMPERATURE MEASUREMENT VERSUS CONDUCTIVITY

During the analysis of the oxygen, fuel, and seed flow rate data the total experimental flow rate (sum of the three flow rates above) was compared with the calculated theoretical total flow rate (from the computer program). It is known that the relation,

$$\dot{M}_{\text{Experimental}} - \dot{M}_{\text{Theoretical}} > 0 \tag{31}$$

is true, but several sets of compared data displayed the contrary. ($\dot{M}$ is the total mass flow rate.)

This variance from the theory was determined to be due to experimental error. This was verified by determining the standard deviation of the experimental total mass flow rate. The standard deviation was determined from like data from three of the four seed concentrations and equations,

$$\hat{\sigma}_{\omega} = \sqrt{\frac{\left(n_1 - 1\right) S_{n_1}^{\ 2} + \left(n_2 - 1\right) S_{n_2}^{\ 2} + \left(n_3 - 1\right) S_{n_3}^{\ 2}}{n_1 + n_2 + n_3 - 3}} , \tag{32}$$

and,

$$S_n^{\ 2} = \frac{\sum_{n=1}^{n} \left(X_i - \overline{X}\right)^2}{n - 1} , \tag{33}$$

where $\hat{\sigma}_{\omega}$ is the standard deviation, n the number of like data runs of the same seed concentration, the subscripts 1, 2, and 3 refer to the seed concentrations 2.5%, 10.5%, and 20.0%, respectively, $S_n^{\ 2}$ the variance, X_i the measured value, and $\overline{X}$ the most probable value. One standard deviation was

determined to be ± 0.042 kilograms per second. Figure 14 displays the experimental total mass flow rate, plus and minus its standard deviation, and the theoretical total mass flow rate. Figure 14 shows that only one data point (Run 557) is above one standard deviation of the experimental total mass flow rate. Therefore, the analyzed data remains consistant with the above mathematical statement (Statement 31).

It was desirable to compare the conductivity measured from the Hall channel with the galvanometer deflections associated with the 7102 and 6655A photomultiplier tubes. Figure 15 graphically displays this comparison which consists of the conductivity versus the normalized percentage of total deflection (100 per cent deflection corresponded to maximum conductivity measured) of the galvanometers. The normalization was required because the galvanometer data points were obtained under two separate galvanometer calibrations. Several calculated least-squares curves were fitted to the data points. The linear least-squares fit was used in the figure and was by far the best fit to the data points. This result apparently meant that the galvanometer deflections increased linearly with the conductivity. The fact that the 6655A tube curve laid above the 7102 tube curve had the significance only that the 6655A tube sensed the same conductivity for a lower percentage of the total galvanometer deflection compared with the 7102 tube.

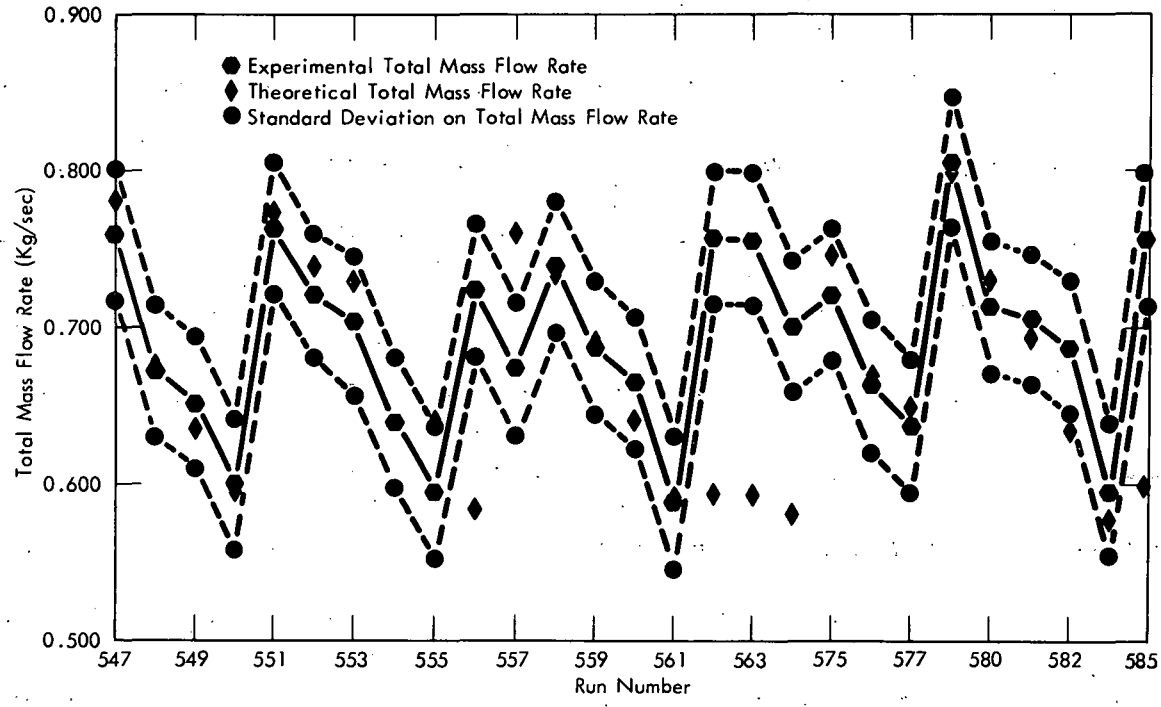

FIGURE 14

COMPARISON OF EXPERIMENTAL VERSUS THEORETICAL TOTAL MASS FLOW RATES

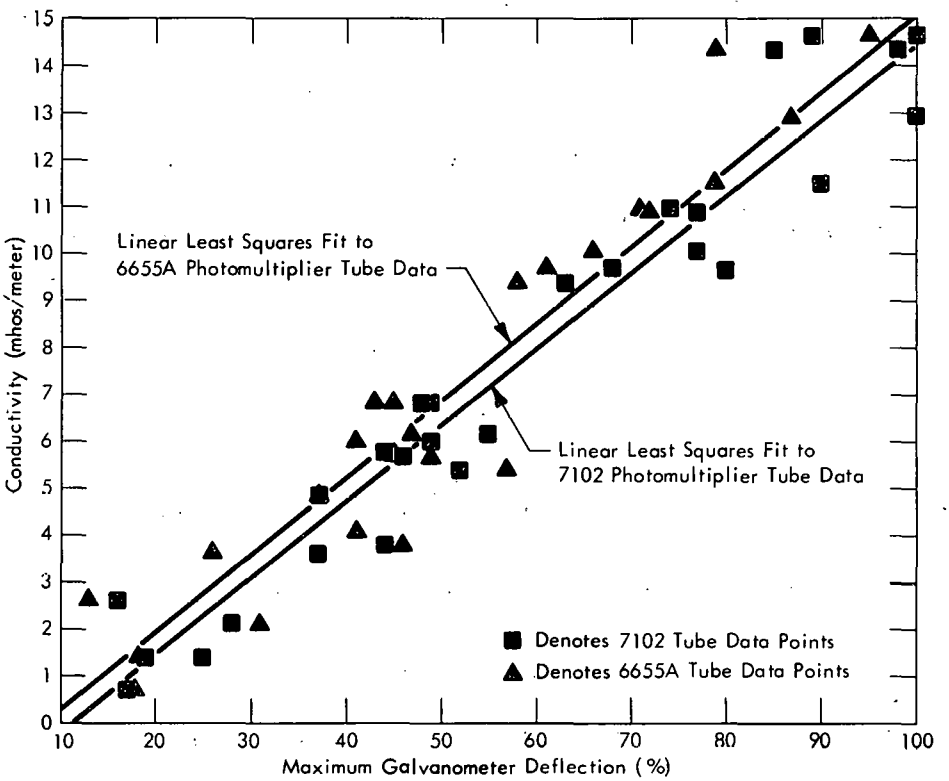

FIGURE 15

CONDUCTIVITY VERSUS THE GALVANOMETER DEFLECTIONS OF THE 7102 AND 6655A PHOTOMULTIPLIER TUBES

Photomultiplier Tube Ratio Temperature Measurement

The photomultiplier tube ratio temperature measurement technique required the ratio of the direct oscillograph galvanometer deflections (in centimeters) of the 7102 and 6655A photomultiplier tubes. This ratio determination was used in conjunction with Equation 25 or 26 to yield the temperature of the MHD plasma. Table IV gives the 7102 phototube galvanometer deflection, the 6655A phototube galvanometer deflection, the ratio of these two deflections, and the temperature of the plasma that was the end result. The experimental data was taken at 10 seconds into the generator test run.

Random Data Analysis

The random data analysis involved the recording, by tape recorder, of the continuous voltage signals of several generator parameters and the two photomultiplier tubes. These voltage signals were continuously recorded throughout each of nine generator test runs and were autocorrelated and crosscorrelated with themselves. The sampling time used for the correlation analysis was 5 seconds. The tape recording of the data was made into a continuous loop and was correlated repeatedly. The parameters that were analyzed included the output of the 7102 phototube, the output of the 6655A phototube, the Hall voltage that existed between Electrodes 20 and 21, and the static pressure that existed at Electrode 22. The voltage outputs of both the 7102 and 6655A

TABLE IV

PHOTOMULTIPLIER TUBE RATIO TEMPERATURE MEASUREMENT DATA

Run Number	7102 Displacement (centimeters)	6655A Displacement (centimeters)	Ratio	Temperature (° K)
547	1.27	1.19	1.09	3043
548	0.91	0.86	1.06	3109
549	0.68	0.51	1.35	2612
550	0.35	0.28	1.27	2722
551	1.37	1.37	1.00	3259
552	1.42	1.40	1.02	3207
553	1.02	0.91	1.11	3000
554	0.68	0.71	0.96	3373
555	0.30	0.25	1.20	2833
556	1.19	1.12	1.04	3157
557	1.85	1.68	1.11	3000
558	1.68	1.52	1.10	3021
559	1.42	1.27	1.12	2980
560	0.91	0.79	1.16	2903
561	0.46	0.35	1.29	2693
562	1.57	1.52	1.03	3181
563	1.85	1.93	0.96	3373
564	1.65	1.81	0.90	3569
575	1.80	1.93	0.93	2320
576	1.47	1.57	0.94	2306
577	0.89	0.84	1.06	2155
579	0.84	0.96	0.87	2415
580	0.96	1.12	0.86	2432
581	0.81	0.91	0.89	2382
582	0.51	0.61	0.83	2487
583	0.30	0.35	0.86	2432
585	0.81	0.89	0.91	2350

photomultiplier tubes were recorded directly by the tape recorder. The tape recorder received the Hall voltage signal through a step-up transformer which was used to isolate, for safety, the recorder from the MHD channel. The static pressure voltage signal was received by the tape recorder from a high-frequency pressure transducer attached and inserted into Electrode 22.

The autocorrelation of the parameters just listed showed that their maximum correlation existed only at $\tau = 0$; therefore, these parameters were not periodic with time. The autocorrelation of the parameters also yielded a numerical dimensionless value at $\tau = 0$ that enabled the normalization of the crosscorrelation function. Both the autocorrelation and crosscorrelation functions were determined by an electronic unit of equipment that was designed for this purpose. Several examples of the data produced by this electronic unit are plotted in Figure 16.

A separate crosscorrelation function was determined on a total of six pairs of parameter voltage signals. These six pairs of crosscorrelated signals consisted of the static pressure versus the 7102 phototube, static pressure versus Hall voltage, static pressure versus 6655A phototube, and Hall voltage versus the 6655A phototube. The normalized crosscorrelation function values for the parameters are summarized in Table V. These crosscorrelation functions were normalized by dividing the value of the crosscorrelation function by the dimensionless value of the averaged two

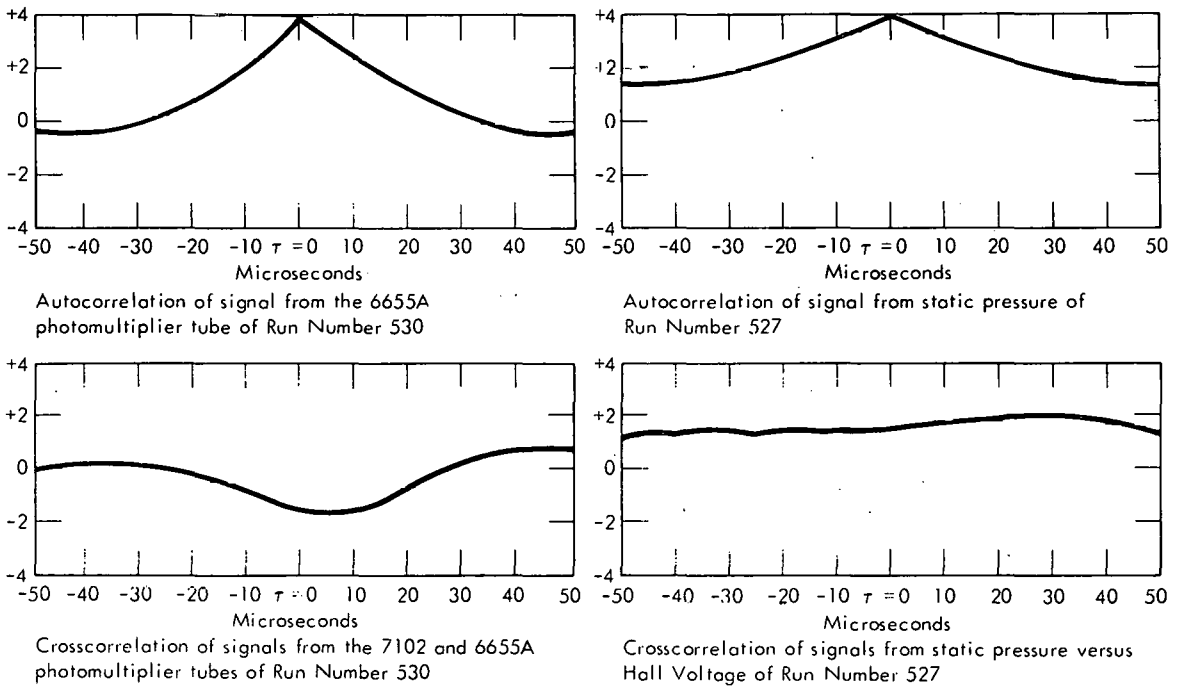

Autocorrelation of signal from the 6655A photomultiplier tube of Run Number 530

Autocorrelation of signal from static pressure of Run Number 527

Crosscorrelation of signals from the 7102 and 6655A photomultiplier tubes of Run Number 530

Crosscorrelation of signals from static pressure versus Hall Voltage of Run Number 527

FIGURE 16

RAW DATA DISPLAY OF AUTOCORRELATION AND CROSSCORRELATION FUNCTIONS

TABLE V

NORMALIZED CROSSCORRELATION FUNCTIONS OF THE MHD GENERATOR AND PLASMA

Run Number	Static Pressure Versus 7102 Tube	Static Pressure Versus Hall Voltage	Static Pressure Versus 6655A Tube	7102 Tube Versus Hall Voltage	7102 Tube Versus 6655A Tube	Hall Voltage Versus 6655A Tube
527	0.026	0.513	0.000	0.051	-0.410	0.077
530	-	-	-	0.077	-0.442	0.052
533	0.103	0.338	0.000	0.182	-0.286	0.158
534	0.053	0.236	0.026	0.105	-0.338	0.052
538	0.105	0.158	0.053	0.158	-0.210	0.131
539	0.053	0.316	0.053	0.053	-0.415	0.052
540	0.026	0.211	0.000	0.105	-0.421	0.079
541	0.105	0.132	0.079	0.158	-0.263	0.131
546	0.105	-	0.105	-	-0.237	-

corresponding autocorrelation functions. A normalized crosscorrelation function equal to unity represented two precisely identical signals. Normalized crosscorrelation functions less than unity represented two signals of varying similarity. Scanning the crosscorrelation data showed that the crosscorrelation functions were of varying degrees less than unity; and, therefore, not a great amount of interdependency existed between the analyzed parameters. The parameters that were the most interdependent were the 7102 phototube versus the 6655A phototube and the static pressure versus the Hall voltage. The meaning of the negative value of the 7102 tube versus the 6655A tube crosscorrelation function could be that one parameter voltage signal was slightly more or slightly less than 90 degrees out of phase with the other. Since this and the other crosscorrelation functions were so low, this negative function may have no meaning.

The spectrums of the fluctuating voltage outputs of both the 7102 and 6655A photomultiplier tubes were analyzed for a characteristic frequency. No characteristic frequency was observed; therefore, the spectral radiance of the plasma varied nonperiodically.

CHAPTER VI

COMPARISON OF TEMPERATURE MEASUREMENT DATA

A comparison of the temperature data of the two different measurement techniques is performed to see what similarities exist. Differences in the temperature measurements obtained by the different techniques are observed and explanations for these differences are developed.

Table VI displays the temperature measurements that are obtained by the conductivity temperature measurement and the phototube ratio temperature measurement.

The conductivity-temperature measurements are used as references to which the other technique data are compared. The conductivity-temperature measurement is chosen as the reference technique due to the fact that this measurement is a theoretical calculation and is the least subject to human error. The main reason for the dissimilarity of the phototube ratio temperature measurements to the reference temperature measurements is the human inability to precisely analyze the raw data required for the ratio calculation.

Since the conductivity-temperature measurement was chosen as the reference measurement it is desirable to compare its data with the raw data from the experimental temperature measurement apparatus; the deflections of the oscillograph galvanometers produced by the photomultiplier tubes.

TABLE VI

COMPARISON OF TEMPERATURE DATA FROM THE DIFFERENT TEMPERATURE MEASUREMENT TECHNIQUES

Run Number	Conductivity-Temperature Measurement (° K)	Photomultiplier Tube Ratio Measurement (° K)
547	2707	3043
548	2532	3109
549	2474	2612
550	2306	2722
551	2717	3259
552	2689	3207
553	2535	3000
554	2514	3373
555	2401	2833
556	2640	3157
557	2656	3000
558	2671	3021
559	2564	2980
560	2527	2903
561	2303	2693
562	2731	3181
563	2734	3373
564	2652	3569
575	2733	2320
576	2670	2306
577	2559	2155
579	2720	2415
580	2707	2432
581	2593	2382
582	2547	2487
583	2455	2432
585	2680	2350

Figures 17 and 18 are plots of the data from the 7102 and 6655A photomultiplier tubes, respectively, versus the conductivity-temperature measurement temperatures. The figures are plotted with the aid of four symbols, each representing a particular seed concentration and grouped together by solid lines. These figures show that the galvanometer displacements increase as the temperature increases.

Since actually the ratio of the phototube displacements is used in the photomultiplier tube ratio measurement technique it is desirable to compare this ratio with the conductivity-temperature measurement. This is performed with the aid of a general equation, known to be applicable because of Equations 25 and 26,

$$T = \frac{3948}{\ln\left[A\, R_a/R_b\right]}\,^{\circ}K \quad , \tag{34}$$

To determine the value of the constant A the form of the above equation that is used is,

$$A = \frac{\mathrm{Exp}\left[\frac{3948}{T_c}\,^{\circ}K\right]}{R_a/R_b} \quad , \tag{35}$$

where T_c is the conductivity-temperature measurement data and R_a and R_b are the 7102 and 6655A tube galvanometer displacements, respectively. A value for A is determined corresponding to each generator test run from which a mean value of A is computed. This results to the equation,

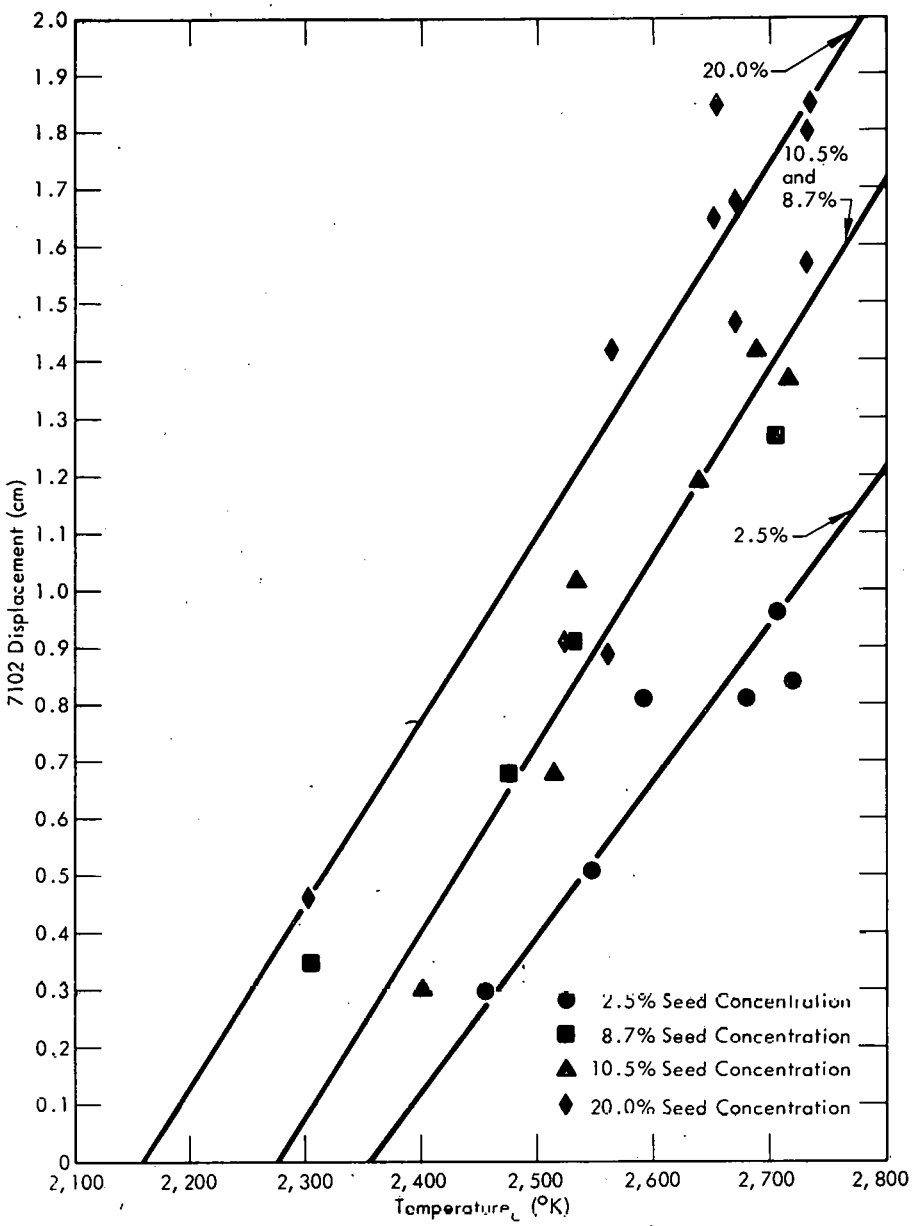

FIGURE 17

7102 TUBE DISPLACEMENT VERSUS THE CONDUCTIVITY-TEMPERATURE MEASUREMENT DATA

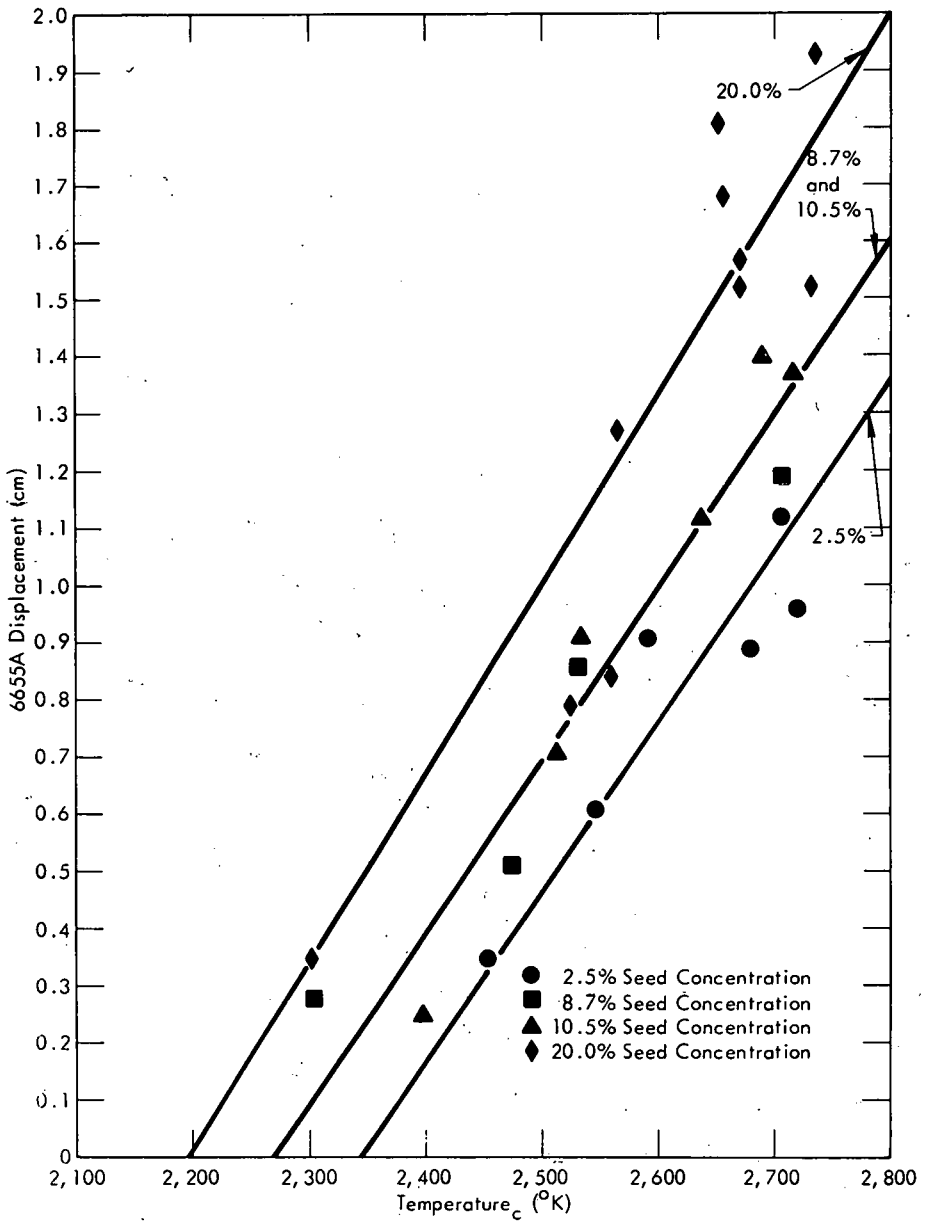

FIGURE 18

6655A TUBE DISPLACEMENT VERSUS THE CONDUCTIVITY-TEMPERATURE MEASUREMENT DATA

$$\ln\left[4.51\ R_a/R_b\right] = \frac{3948^\circ K}{T_c} \quad . \tag{36}$$

The above relation permits the comparison between the ratio R_a/R_b and T_c. Figure 19 is a plot of the left side of the above equation versus the right side. The solid line is a linear least squares fit to the data. The dotted lines show plus and minus one standard deviation which is ± 0.132.

The oxygen-fuel flow rate ratio was indirectly varied to change the temperature of the plasma during a test run. A comparison of these parameters is interesting and is plotted in Figure 20. The solid symbols in the above mentioned figure represent data corresponding to the conductivity-temperature measurement and are connected by means of a solid curve which is a least squares parabolic fit to the data. This data shows for the conductivity-temperature measurement that generally as the oxygen-fuel flow rate ratio decreases so does the temperature.

An interesting comparison is displayed in Figure 21 between the combustor loss and the data from the conductivity-temperature measurement. The combustor loss decreases as the temperature decreases.

All of the test runs are analyzed to determine if they existed under stoichiometric conditions or what were their fraction of stoichiometric. What fraction of stoichiometric is determined by the equation(14),

$$\epsilon = \frac{\dot{M}_O/32}{0.1062\ \dot{M}_K + \dot{M}_S(1-f_{KOH})/15.356} \tag{37}$$

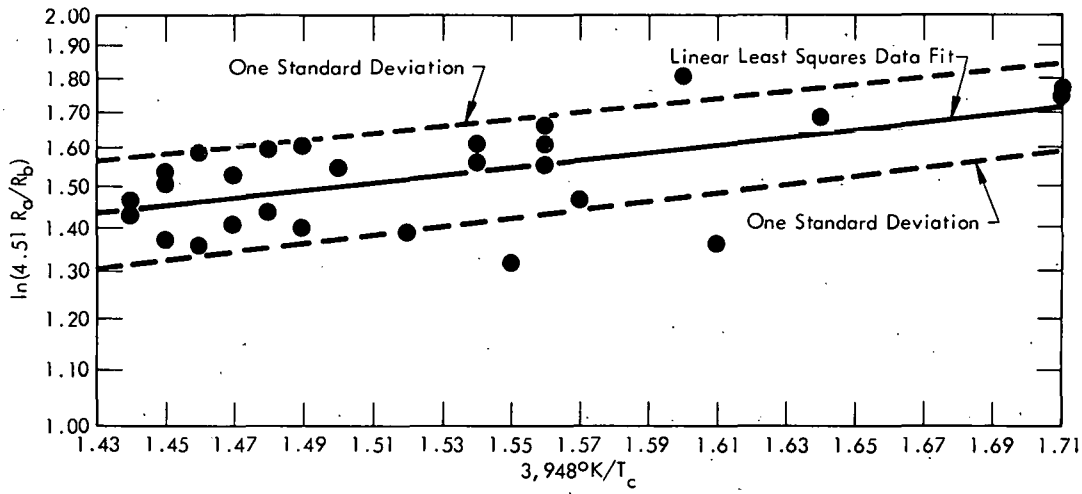

FIGURE 19

COMPARISON OF THE PHOTOTUBE DISPLACEMENTS RATIO VERSUS THE CONDUCTIVITY-TEMPERATURE MEASUREMENT

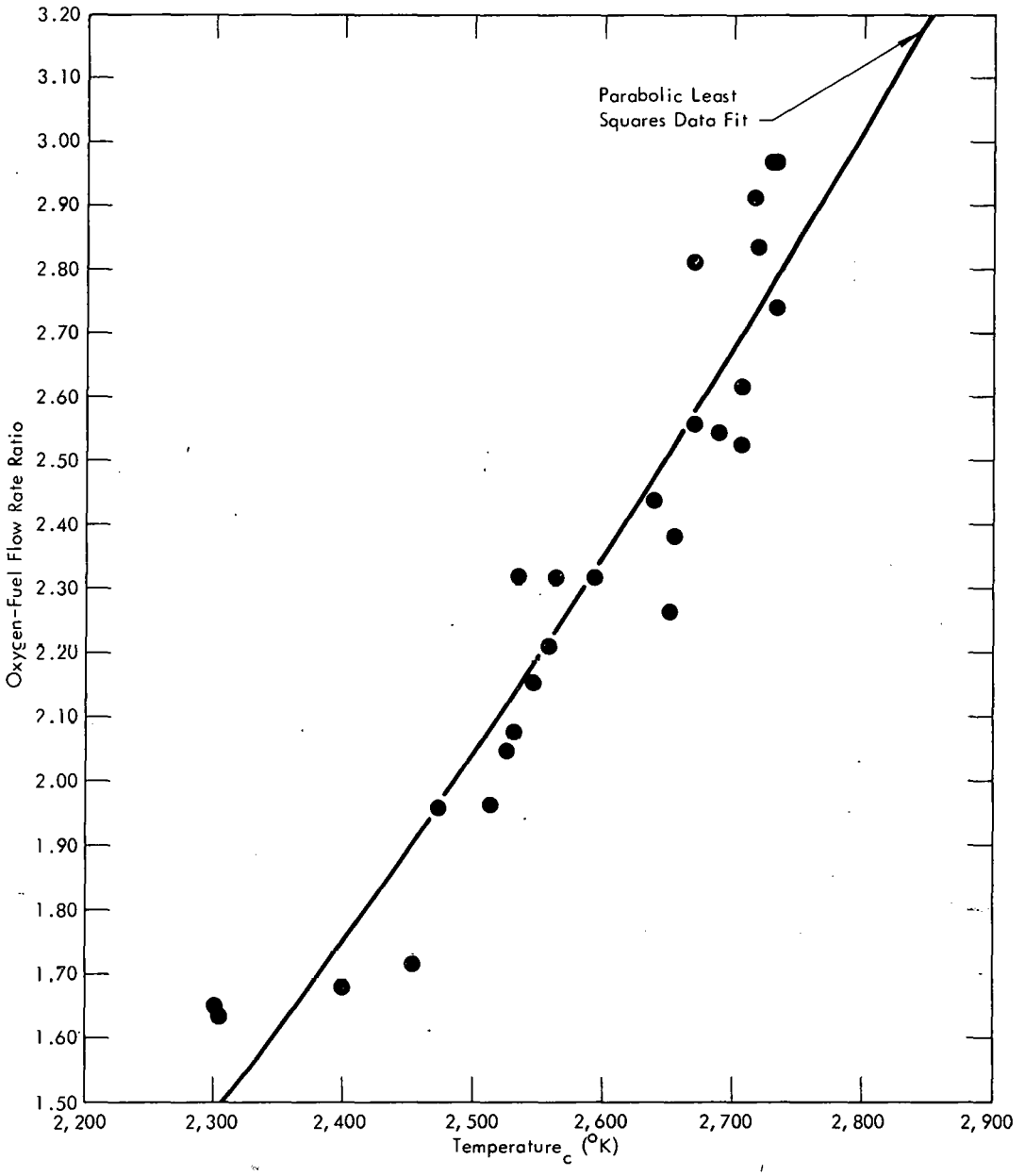

FIGURE 20

COMPARISON OF THE CONDUCTIVITY-TEMPERATURE MEASUREMENT DATA VERSUS THE OXYGEN-FUEL FLOW RATE RATIO

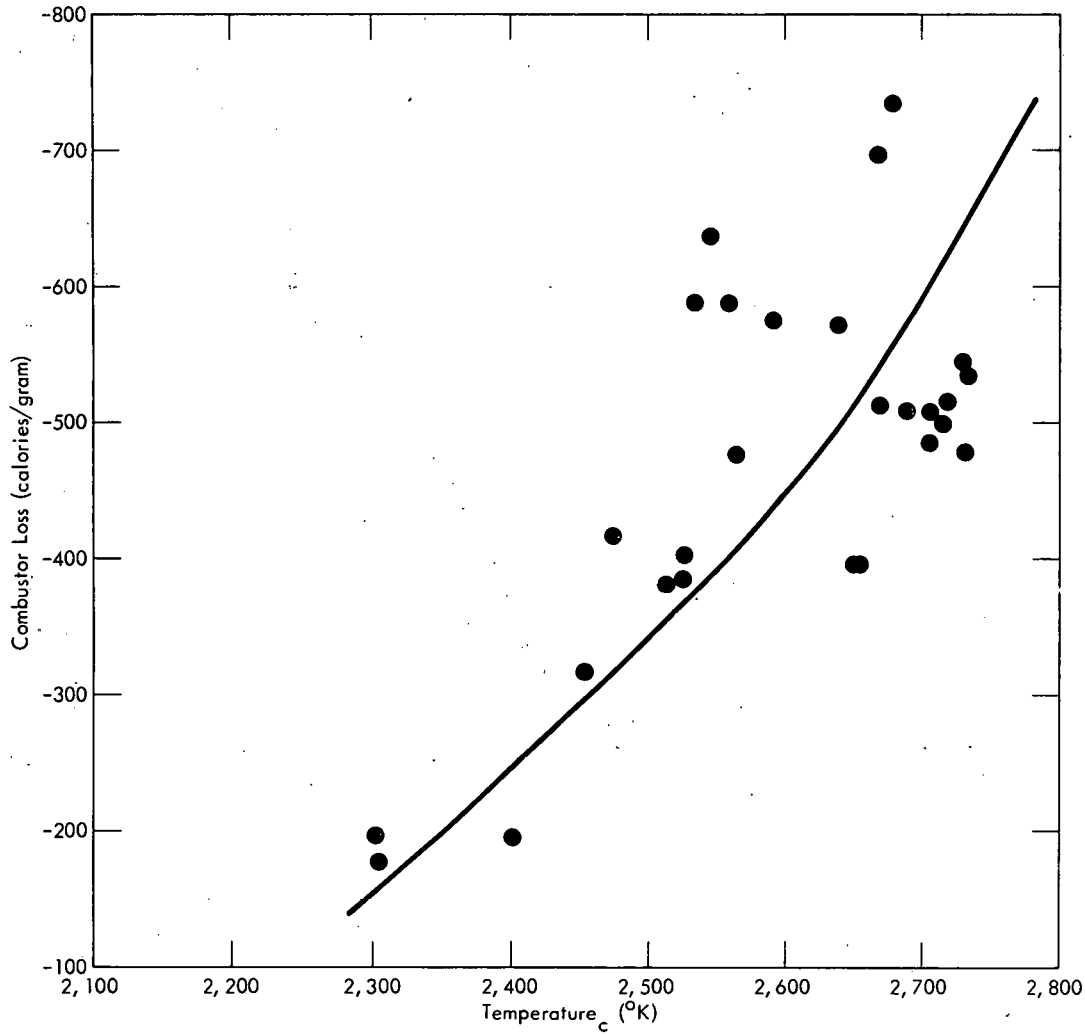

FIGURE 21

COMBUSTOR LOSS VERSUS TEMPERATURE

where $\dot{M}_O$ is the oxygen flow rate, $\dot{M}_K$ is the kerosene flow rate, $\dot{M}_S$ is the seed flow rate, and f_{KOH} is the seed fraction. Figure 22 is a plot of the combustor loss versus the fraction of stoichiometric for each of the test runs. This figure shows that none of the test runs existed under stoichiometric conditions and that as the fraction of stoichiometric decreased so did the combustor loss.

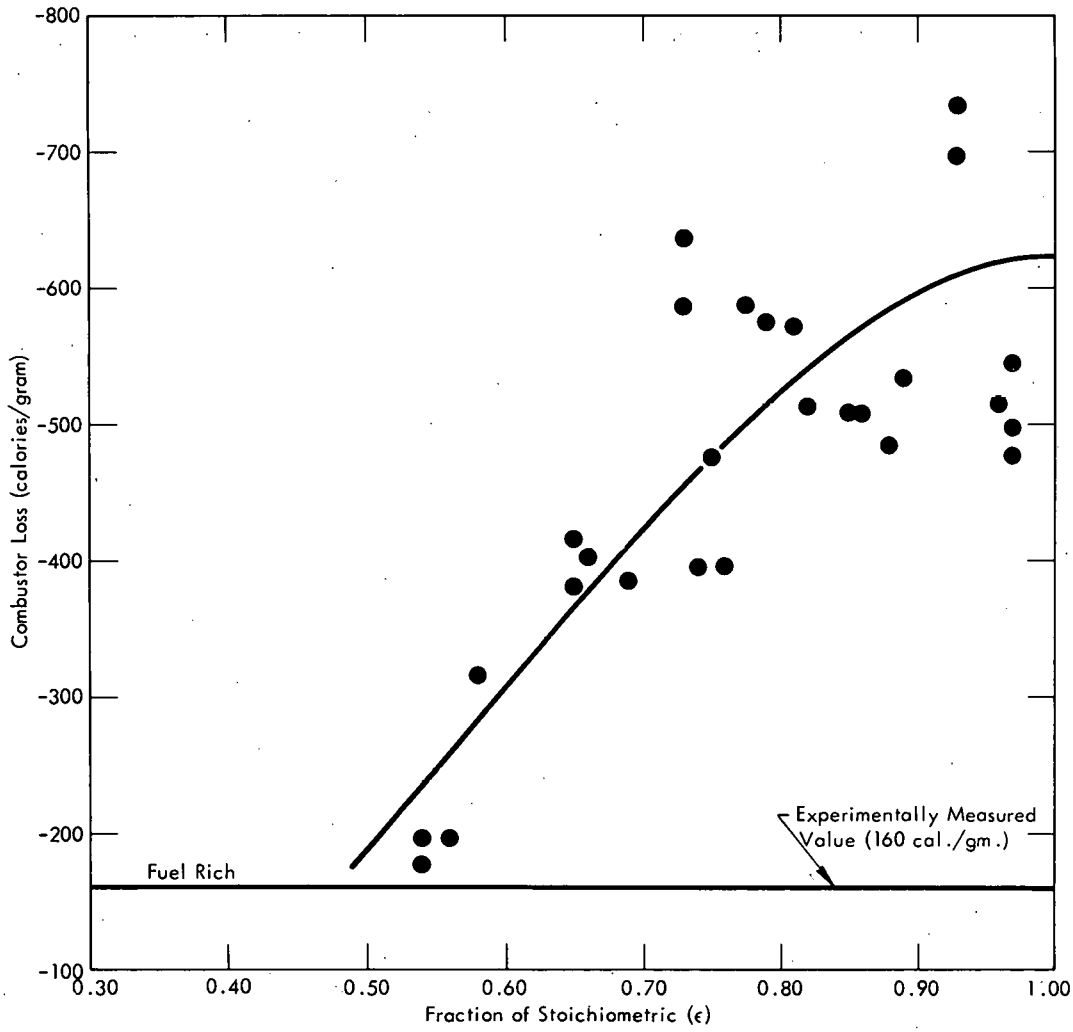

FIGURE 22

COMBUSTOR LOSS VERSUS FRACTION
OF STOICHIOMETRIC

CHAPTER VII

CONCLUSIONS AND RECOMMENDATIONS

The principal conclusion from this work is that the photomultiplier tube temperature sensing apparatus worked well and yielded useful information in several respects. This apparatus has the potential to yield useful plasma temperature measurements. The temperature measurement accuracy as of now is not as good as expected due to several reasons. The autocorrelation and crosscorrelation of several of the generator parameters yielded information that was previously unknown.

There exists a high fluctuation in the intensity of the KI lines which means there is a fluctuation of the plasma temperature. Spectrum analyses of the recordings of the raw photomultiplier tube data establishes that these KI line fluctuations are not periodic, but appear to be white random noise. These KI line fluctuations are entirely uneffected by the absolute temperature of the plasma (these fluctuations exist whether the plasma temperature is 2300 or 2700 degrees Kelvin).

The temperature measurements of the experimental temperature measuring device are adversely affected because of the inability to precisely analyze the raw data from the oscillograph charts. This is due to the fact that the data on the oscillograph charts are clustered (each individual voltage peak

is not distinguishable). The temperature measurements from the experimental apparatus are adversely affected also by the fogging of the optical window between the plasma and the phototubes. Finally, the temperature measurements are adversely affected, shown by the experimental error associated with the total mass flow rate and temperature parameters, due to the inability to precisely preset and maintain the total mass flow rate parameters. This aids in the production of the high voltage peak fluctuations displayed on the oscillograph charts. The temperature measurement is not determined directly from the measurement apparatus, but indirectly from data from the oscillograph charts which corresponds to voltage output from the photomultiplier tubes.

Recommendations to improve the temperature measurements are: The ability to precisely analyze the raw data from the oscillograph charts is possible by increasing the speed of the chart paper advance of the oscillograph. This procedure would make each voltage peak distinguishable. The adverse affect of the fogging optical window can be controlled by increasing the flow rate of the argon purge and by replacing the optical window after each or several generator test runs. The ability to precisely preset and maintain the total mass flow rate of the oxygen, seed, and fuel is by far the most difficult to improve. The utilization of a liquid oxygen rather than a gaseous oxygen system may improve the situation.

Performing autocorrelation and crosscorrelation on the parameters of chamber pressure, Hall voltage, 7102 phototube output, and 6655A phototube output, showed, in conclusion, that, statistically, they are not interdependent.

THIS PAGE

WAS INTENTIONALLY

LEFT BLANK

LIST OF REFERENCES

1. Manual, C., and N. W. Mather. Engineering Aspects of Magnetohydrodynamics. New York: Columbia University Press, 1962.

2. Dicks, J. B., and Ying-chu Lin Wu. "Diagonal Conducting Wall Generators." Report prepared under Contract AF 33(615)-2691 by The University of Tennessee Space Institute, Tullahoma, Tennessee, January, 1967.

3. Simmons, F. S. "Spectroscopic Pyrometry of Gases, Flames, and Plasmas," ISA Transactions, II (April, 1963), 168-189.

4. Edmund Catalog 701. Barrington, New Jersey: Edmund Scientific Co, 1969.

5. Martin, J. F. "Current Distribution in a Hall Generator Electrode." Unpublished Master's thesis, The University of Tennessee, Knoxville, 1970.

6. Edwards, L. W. "Aluminum-RP-1 Mixtures as High Performance Fuels for MHD Power Generation." Unpublished Master's thesis, The University of Tennessee, Knoxville, 1970.

7. Frost, L. S. "Conductivity of Seeded Atmospheric Pressure Plasmas," Journal of Applied Physics, XXXII (October, 1961), 2029-2036.

8. Crawford, L. W. Private communication. The University of Tennessee Space Institute, Tullahoma, Tennessee, November, 1970.

9. Rocketdyne Division of North American Aviation, Inc. "Emissivity of Tungsten versus Wavelength from Ultraviolet to Near Infrared Region for 1600-2400°K Temperature Range," Rocketdyne Research Report No. 59-32, Canoga Park, California, June, 1959.

10. Olsen, H. N., G. Bedjai, and F. L. Kelly. "Development of Diagnostic Methods for Seeded Air and Nitrogen Plasmas." Report prepared under contract F 40600-67-C-0017 by Plasma Sciences Laboratories, Inc., Van Nuys, California, December, 1968.

11. Grober, H., and S. Erk. Fundamentals of Heat Transfer. New York: McGraw-Hill Book Company, Inc., 1961.

12. Koester, J. K. Private communication. The University of Tennessee Space Institute, Tullahoma, Tennessee, August, 1970.

13. Bendat, J. S., and Allen G. Piersol. Measurement and Analysis of Random Data. New York: John Wiley and Sons, Inc., 1966.

14. Crawford, L. W. Private communication. The University of Tennessee Space Institute, Tullahoma, Tennessee, August, 1971.

VITA

Edward Michael Murray was born in Norfolk, Virginia on January 8, 1946. He attended an elementary school in that city and was graduated from Granby High School in 1964. The following September he entered Old Dominion College in Norfolk; and, in June 1968, received a Bachelor of Science degree in Physics. After graduation, he was employed by Union Carbide Corporation-Nuclear Division in Oak Ridge, Tennessee. In the summer of 1969 he accepted a research assistantship at The University of Tennessee Space Institute having first been granted a leave of absence from Union Carbide. There he began study toward a Master of Science degree in Physics. In November 1970 he resumed employment with Union Carbide.

He is a member of Sigma Pi Sigma. His wife is the former Harriet P. Watson of Virginia Beach, Virginia.